



A few perspectives of solar physics research in China - current status and future

Jingxiu Wang^{1*}, Mingde Ding^{2*}, Haisheng Ji^{3*}, Yuanyong Deng¹, Yu Liu^{1,4}, Zhong Liu^{1,4},
Zhongquan Qu^{1,4}, Huaning Wang¹, Lidong Xia⁵ and Yihua Yan¹

¹Key Lab of Solar Activity, National Astronomical Observatories, Chinese Academy of Sciences, Beijing, China

²School of Astronomy and Space Science, Nanjing University, Nanjing, China

³Key Lab of Dark Matter and Space Astronomy, Purple Mountain Observatory,
Chinese Academy of Sciences, Nanjing, China

⁴Yunnan Observatories, Chinese Academy of Sciences, Kunming, China

⁵School of Space Science and Physics, Shandong University, Weihai, China

Solar physics research as an important discipline in astrophysics in China aims at improving the understanding of origin and variation of solar magnetic field and magnetic activity, and founding the basis for forecast of disastrous space weather. The current review is focused on the solar physics research in China in recent three years. Highlights in scientific research in solar magnetism, magnetic activity, coronal plasma, and space weather forecast are briefly summarized. Key advances in instrument development are reported in some necessary details. Future tendency and working direction are considered and discussed © Anita Publications. All rights reserved.

Keywords: Sun: activity; Sun-magnetic fields; solar wind; site testing; telescopes

1 Introduction

Solar physics research has gained an important position in Chinese astronomy and astrophysics. It is one of the astrophysical disciplines in China with heavy and active studies, which are mostly focused on understanding the origin and variation of solar magnetic field and magnetic activity. The ultimate goal of the solar physics studies in China is to gain the capability of predicting the violent solar activity and disastrous space weather from the near-Earth environment throughout the heliosphere. As for the only star which can be observed with high tempo-spatial and spectral resolution and polarization accuracy, Chinese solar astronomers put their work in the frame of general astrophysics with the emphasis on the physical processes of radiation magneto-hydrodynamics (RMHD) and plasma physics.

Solar physical studies in China are concentrated in the four key institutes of Chinese Academy of Sciences (CAS) and five national universities. Among them, there are a Key Lab of Solar Activity located in the National Astronomical Observatories (NAOC, Beijing) of CAS, a State Key Lab of Space Weather in the National Space Science Center of CAS, a few sizable research groups in Yunnan Observatories (YNAO, Kunming) and Purple Mountain Observatory (PMO, Nanjing) of CAS, School of Astronomy and Space Science of Nanjing University (NJU, Nanjing), School of Earth and Space Sciences of Peking University (PKU, Beijing) and the University of Science and Technology (USTC, Hefei), and School of Space Science and Physics of Shandong University in Weihai (SDU, Weihai), and Astronomy Department of Beijing Normal University (BNU, Beijing). Very recently, the National Observatory for Space Weather of China Meteorological Administration (CMA) was established. It is responsible for the monitoring, warning and predicting of disastrous space weather and organizing the relevant scientific work. New initiatives in

Corresponding authors :

e-mail: wangjx@nao.cas.cn (Jingxiu Wang); dmd@nju.edu.cn (Mingde Ding); jhs@pmo.ac.cn (Haisheng Ji)

heliophysics studies have also been founded in a Key Lab of Earth and Planetary Physics of CAS in the Institute of Geology and Geophysics. More than five hundreds of professors, scientists, engineers and Ph.D. students are engaged in solar physics research in these organizations.

In the late of 1980s Solar Magnetic Field Telescope was invented and set up in operation at Huairou Solar Observing Station of NAOC [1]. Many thousands of solar active regions have been mapped with magnetographs at both the photosphere FeI 532.4 nm and chromosphere H β 486.1 nm lines and their vector magnetic fields been measured in the photosphere [see, 2, 3], flourished studies on solar magnetism and activity have been carried out since then. Together with the observations of the multiple solar spectrographs and the physical diagnosis of sunspots, solar flares and filaments at PMO, YNAO, and NJU [see, 4-7], dynamic growth of solar physics studies were witnessed in China. The growing trend has been continued until now.

Two previous reviews on Chinese solar astronomy have covered the literature roughly from 2006 to 2012 [8, 9]. Therefore, the emphasis of the current review is put on the most recent research since 2013. We will first highlight the scientific researches on solar magnetism, activity, coronal heating and solar wind acceleration, and space weather forecasting, and then we report the current status of the key projects which have been formally founded. In the last section, we present the considerations on the future direction and efforts.

2 Highlights in scientific research

2.1 Solar magnetism

Observations with the Solar Magnetic Field Telescope have fostered the growth of research groups of solar magnetism and magnetic activity, which become a favorite working direction in Chinese solar astronomy. More advanced space observations of the Sun's magnetic fields by Hinode/SP, SOHO/MDI and SDO/HMI have encouraged further efforts in learning the properties of magnetic fields on the quiet Sun and in active regions (ARs), the magnetic non-potentiality and helicity in relation to solar eruptions, the solar cycle behavior of magnetic flux in the flux spectrum from tiny intranetwork to AR fields, and in understanding the unusual low activity level in the Grand Minima of Solar Cycles 23–24. Chinese authors contributed approximately 10% papers in solar magnetism and magnetic activity studies in last 3 years.

2.1.1 Three-dimensional theoretical extrapolation and simulation

It is commonly believed that the primary magnetic energy release in solar activity takes place in the corona. However, the magnetic properties in the corona are poorly known. Getting along with the international solar physics community, Chinese solar astronomers have made important progress in 3D theoretical extrapolation from the observed vector magnetic fields on the solar surface to the corona, based on the assumption of non-linear force free field (NLFFF) in the upper solar atmosphere. In addition to the extrapolation, to learn the magnetic field in the chromosphere and transition region becomes an important task, as the magnetism in these layers are least known; Moreover, their role in transporting the magnetic energy and complexity to the corona is crucial for solar activity.

Jiang and Feng introduced a method based on CESE-MHD model with the conservation- element/ solution-element (CESE) space-time scheme [10]. They developed a CESE-MHD-NLFFF code and applied it to the observed vector magnetic field in the photosphere, obtained by SDO/HMI. The reconstructed magnetic field lines in ARs were found to match the observed EUV intensity structures shown by SDO/AIA very well. More interestingly, they were able to reconstruct the strongly sheared magnetic lines of force suspending the filaments and the twisted flux ropes corresponding to the sigmoidal structure in flare-productive ARs. More detailed comparison between the reconstructed magnetic structures and the observed intensity structures were presented in the follow-up papers [11, 12].

Wang *et al* developed a GPU-accelerated direct boundary integral equation (DBIE) method and applied it to the observed vector magnetograms to reconstruct the 3D coronal magnetic structure of AR11158 [13]. It is found that the GPU-accelerated method was 1000 times faster than an original DBIE. The direct boundary integration method has an advantage in release of an artificial constraint of zero-net-flux on the boundary, which is required by most of the NLFFF extrapolation methods.

Although NLFFF model could be used to excellently reconstruct the 3D magnetic structures in the corona, which resemble the observed EUV intensity structure very well, the extrapolation, in principle, is only valid for some quasi-equilibrium field. To understand the real mechanism or mechanisms of solar explosive activity, we need to learn the more realistic evolution of the 3D field. However, a very good strategy is to use the reconstructed 3D magnetic structure as the initial condition in a MHD or RMHD simulation. Jiang *et al* take the advantage of their CESE-MHD-NLFFF reconstruction and put their NLFFF into a 3D MHD simulation for a better understanding the physics of magnetic eruption in AR11283 [14]. These authors were able to identify a magnetic null in the envelope of the sigmoid core, and find that the magnetic reconnection at the magnetic null triggered the torus instability of the flux rope for the magnetic eruption in this AR.

The 3D NLFFF modeling and MHD simulation are mostly referring to an AR or a rather small area on the Sun. However, for an eruption event, often two or more ARs are connected and serve as the real magnetic source. Wang *et al* demonstrated with 3 clusters of ARs that quite a few flare/CME events were initiated from the instability of either the AR-connecting magnetic loops or the channeling filament between two ARs [15]. Modeling the magnetic connectivity between two or more ARs would help greatly with exploring the mechanism of complex eruption events.

Jin *et al* analyzed the daily full-disk magnetograms taken at Ca II 854.2 nm from the Synoptic Optical Long Term Investigations of the Sun (SOLIS) facility to study the chromospheric magnetic field from 2006 April through 2009 November [16]. Synoptic maps of the chromospheric radial flux density distribution were constructed and used as boundary conditions for extrapolation of the field from the chromosphere into the corona. The authors compared the modeled and observed locations of coronal hole and coronal streamer locations, found a better agreement when using the chromospheric rather than the photospheric synoptic maps for the extrapolation.

2.1.2 Magnetic helicity

Magnetic helicity is an important physical quantity. It, on one hand, maintains necessary information on the physics of magnetic field generation. Therefore, it provides a diagnosis of the field generation. On the other hand, defined by the projection of magnetic field on its vector potential, magnetic helicity represents the complexity of field geometry. Phenomenologically, for a flux system with ideal magnetized fluids, the total helicity in a volume is a topology invariable which constrains the minimum magnetic energy status in the system. As a well-known case, the minimum energy status for a magnetic flux system is a linear force free field if the total helicity does not change with time.

Yang *et al* developed a new method to calculate the vector potential of magnetic field in a finite volume [17]. By using a fast Laplace/Poisson solver, the method can obtain the vector potentials for a given magnetic field and for the corresponding potential (current-free) field. Accordingly, the relative magnetic helicity can be calculated. The method was applied to the 3D magnetic field above AR8120 obtained by a photospheric-data-driven MHD model. Not only the calculated relative helicity changes were found consistent with the relative helicity inflow from the boundary in the ideal and non-ideal cases, but also the correlation of magnetic helicity accumulation with the onset of flare activity was confirmed. The maximum relative helicity of 0.0298 normalized by the total flux was identified for the AR right before the onset of a major flare.

Zhang *et al* for the first time obtained the magnetic energy and helicity spectra by using the observed photospheric vector magnetic field for an AR [18]. They found that at all wavelengths the helicity sign

agreed with the hemispheric law predicted theoretically. The magnetic helicity normalized by the maximum theoretical value reached 0.04 and became strongest at the wavenumber corresponding to the spatial scale of 16 Mm. Either the energy spectrum or the current helicity spectrum showed modulus of a power law of $K^{-5/3}$, indicating turbulent nature. With regarding to the long term evolution, Zhang and Yang [19] found a consistency in changes between the total injected magnetic helicity and the sunspot number in a statistical sense (see Fig 1). Their estimation seemed to only come from the stronger field in ARs, however, the problem is that even in the minimum phase of the cycle, some big CMEs ejected enough magnetic helicity into the interplanetary space. The huge amount of helicity might be injected by the eruption of some large filaments in the Sun's quiet region or at the boundary of coronal holes. The magnetic field in the cycle minimum phase might be weak, but was organized into some large-scale patterns which should contain enough helicity. Zhang and Yang [19] estimated a total injection helicity of $5 \times 10^{46} \text{ Mx}^2$ in the 23rd solar cycle.

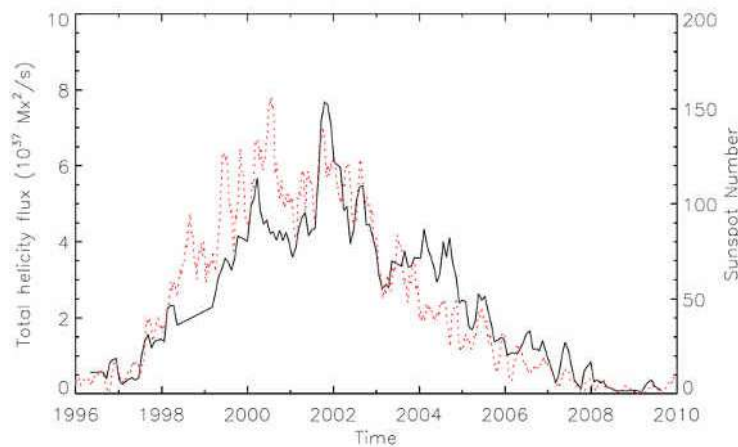


Fig 1. Total magnetic helicity flux (solid line) and sunspot numbers (dotted) line in 1996-2009.

It is realized that for getting accurate determination of magnetic helicity, utilizing the vector magnetic field observations is of great importance. Song and Zhang investigated the effects of non-radial magnetic field in calculating the helicity injection rate for ARs [20]. They found that by only using the line-of-sight component of magnetic field, the helicity injection rate could not be correctly estimated for the ARs which located close to the limb. Song *et al* studies the evolution of electric current, current helicity, source field, photospheric free magnetic energy, and magnetic shear angle for a flare-productive region, AR11158 [21]. They further confirmed that comparing to magnetic flux, the magnetic non-potentiality and complexity are more closely associated to flare/CME activity.

2.1.3 Solar cycle in term of flux spectrum

Solar cycle is defined originally from the variation of sunspot numbers. However, sunspots only represent the strong component of solar magnetic field which, in fact, exhibits a hierarchy from the smallest weak intra-network (inter- or inner-network, abbreviated as IN) elements to the fields of network (NT), plage, pores and sunspots with gradually increased size, flux and field strength. To understand the solar magnetism, the knowledge of magnetic flux spectrum and its changes in a solar cycle are urgently needed.

Jin and Wang studied the long-term variation of solar magnetic flux spectrum and its characteristics in the grand minima in solar cycles 23-24, based on the full-disc SOHO/MDI magnetograms covering the interval of 1996-2011 [22]. They used a way of automatic feature detection in this and later approaches in identifying many million elements of magnetic flux ranging from intra-network to ARs to make their results solid. They found that the extended minimum in Cycle 23 was characterized by the minimum activity level

defined by a long duration of low activity and minimum number of sunspots. However, the magnitude of magnetic flux in this period is not lower than previous cycle as the component of quiet network which was anti-correlated to the sunspot number contributed enough magnetic flux during the deep minimum [23]).

From a statistical point of view Li *et al* evaluated various activity proxies in term of the closeness in correlation with solar magnetism [24]. They recommended that the most representative index for the weak magnetic activity would be the 10.7 cm radio flux, while the most representative index for the strong magnetic activity would be the sunspot area.

Magnetic flux distribution of intra-network field has been quantified with the data from the Narrow-band Filter Imager of Solar Optical Telescope (SOT/NFI) on board of Hinode [25]. The flux distribution of IN and NT field peak at $(1-3)\times 10^{16}$ Mx and $(2-3)\times 10^{17}$ Mx, respectively. The IN field alone contributes 52% of the total solar flux and 12.3 G flux density to the Sun at any given time. By taking the 3 minute lifetime of IN elements [26] into account, the IN elements provide 3.8×10^{26} Mx to solar surface per day. Such a huge contribution makes the studies of IN field source and cyclic evolution urgently important.

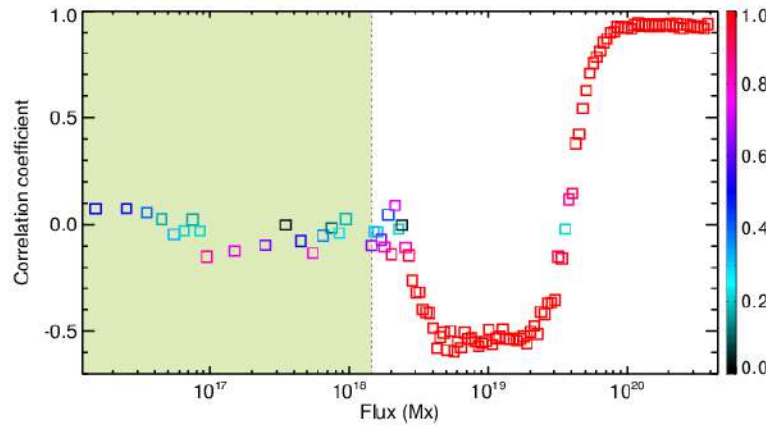


Fig 2. Correlation of the flux variation of magnetic elements in the flux spectrum from 10^{16} to 4×10^{20} Mx with sunspot number changes: the right unshaded part is constructed from Solar Cycle 23, based on the SOHO/MDI full-disc magnetograms; the left shaded part is calculated from flux density of IN elements, based on the Hinode SOT/SP data in the interval of 2007 – 2014 [27]. The flux density of IN elements with flux less than 10^{18} Mx does not show correlation with sunspots numbers. The right vertical bar represents the confidence level of the correlation. Sunspot numbers were taken from the International Sunspot Number.

By the advances in spatial resolution and polarimetry sensitivity, the Hinode solar spectropolarimetry data (SOT/SP) in the period from the minimum to maximum of current solar cycle opens an unprecedented opportunity to study the cyclic behavior of IN field. Jin and Wang conducted a group of studies on how the variations of IN magnetic flux and horizontal field correlate to the changes of sunspot numbers and what are the changes of IN magnetic field in the solar cycle [27, 28]. With substantial sets of data, Jin and Wang concluded that either the vertical or the horizontal IN field did not follow the variation of sunspot numbers, i.e., the activity levels (see Fig 2). From the minimum to the maximum of Cycle 24, the average flux densities of IN vertical and horizontal fields were 10 ± 1 G and 87 ± 1 G, respectively, so that the imbalance between horizontal and vertical field maintained at the level of 8.7 ± 0.5 in the duration from the solar minimum to the maximum. The results appear to support an idea that the solar IN field originates from a locally small-scale dynamo. IN field does not seem to come from the diffusion and/or recycling of AR flux; that is to say, it does not seem to join the general dynamo which underlines the sunspot cycle.

2.1.4 Understanding and predicting of solar cycle

In the last solar cycle there were two groups of authors who made first solar cycle prediction based on the flux transport dynamo model [29-31], which makes a milestone in the solar cycle studies. The main difference lies in the treatments of the surface poloidal field source and the unknown parameters of the convective zone, i.e., the magnetic diffusivity and the meridional flow. The prediction on the activity level of Cycle 24 made by Choudhuri *et al* and Jiang *et al* was well proved by the real progress of the cycle [30-31].

To investigate the essence of the solar cycle, Jiang *et al* modeled solar cycles 15 to 21 by adopting a flux transport dynamo model including convective pumping and a poloidal source term from the historical record of sunspot group areas, locations, and tilt angles [32]. These authors found evidence that the polar fields near cycle minima and the toroidal flux at the base of the convection zone were highly correlated with the subsequent maxima of solar activity. The behavior of the Babcock-Leighton dynamo shows the consistency with the observationally inferred correlations. This indicates that the Babcock-Leighton mechanism is at the heart of the solar cycle.

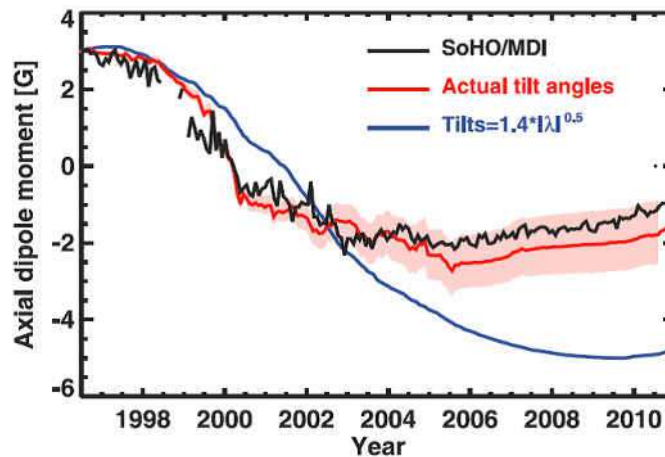


Fig 3. Evolution of the solar axial dipole moment [33]. The curves correspond, respectively, to observed SOHO/MDI magnetograms (black), a simulation using the actual tilt angles of bipolar magnetic regions (red, hence the contribution of the abnormal ones is included), and a simulation using tilt angles according to a fitted latitude dependence (blue, which is the usual way to deal with the tilts).

An important revelation was made by Jiang *et al* [34]. They claimed that the tilt angles of sunspot groups play a crucial role in the build-up and reversals of the polar fields thus, for a practical prediction of the activity level of subsequent cycle (see Fig 3). They described the scatter of sunspot tilt angle in their surface flux transport (SFT) simulation by a random component according to the observed distributions of sunspot group size. By selecting three solar cycles with weak, medium, and strong activity levels, respectively, in performing the SFT simulation, they discovered that the effect of the scatter of sunspot tilt would cause a clear uncertainty in modeling of the Sun's global magnetic field in term of the axial dipole moment [see also a review, 35]. Very recently, Jiang *et al* further identified that weak polar fields in the previous cycle minimum and thus the weakness of current cycle were mainly resulted from a few bigger bipolar regions emerged at low latitudes in last solar cycle, with a “wrong” tilt angle that impaired the growth of the polar field [33].

Solar differential rotation is one of the intrinsic physical processes, which lead to the generation of Sun's magnetic field and its cyclic variation. The studies of solar differential rotation so far are largely depending on statistical investigations. Li *et al* revisited the long-term variation of solar differential rotation

with substantial sets of data [36]. They found that the solar-surface-rotation rate at the equator showed a secular decrease from Cycle 12 onwards, and the latitude gradient of differential-rotation seemed to show a secular decrease too since Cycle 12 onwards with relatively weak statistical significance. Moreover, these authors revealed that the average sunspot area exhibited a secular increase of statistical significance since Cycle 12 onwards; and a negative correlation between the level of sunspot activity (indicated by the average sunspot area) and the solar equatorial rotation on long-term scales was identified. Li and his co-workers also studied the in-cycle variation of solar differential rotation statistically and obtained interesting results [37, 38].

2.2 Solar active events: observations and modeling

2.2.1 Observations of magnetic reconnection, flux rope and coronal mass ejections

Magnetic reconnection refers to a change of magnetic field connectivity and is believed to be a fundamental energy release process in various astrophysical phenomena. However, this process is difficult to observe directly. By adopting the observed H α , UV, EUV, or X-ray structures as the proxies of magnetic lines of force, we can get indications of magnetic reconnection – position, scenario, and consequence. Many interesting studies have been made by Chinese authors in this working direction.

Using the high tempo-spatial resolution H α images provided by the New Vacuum Solar Telescope (NVST), Yang *et al* presented observational indications of magnetic reconnection that occurred between two sets of small-scale, anti-parallel loops [39]. Using the combined perspectives of two spacecraft, Sun *et al* reconstructed the three-dimensional (3D) magnetic topology of a reconnection event [40]. The results show that two groups of oppositely directed magnetic loops gradually approach each other and reconnect, providing direct evidence of magnetic reconnection in 3D. The reconnection process changes the ambient magnetic fields from open loops to closed post-flare ones as seen in many flares [41].

Recently, the slipping running reconnection has attracted much attention. Li and Zhang studied a flare that occurred on 2014 February 2 and found that the east flare ribbon moved with a slipping motion at a velocity of 50 km s⁻¹ lasting about 40 minutes, while the west flare ribbon propagated in the opposite orientation with a velocity of 30 km s⁻¹ [42]. Through examining an eruptive X-class flare on 2014 September 10 by Interface Region Imaging Spectrograph (IRIS) observations, Li and Zhang further discovered the quasi-periodic behavior of the slipping reconnection that evolved along one of the two ribbons during the impulsive phase of the flare [43]. The apparent slipping speed was 20-110 km s⁻¹, and the corresponding period was 3-6 minutes.

Magnetic flux rope (MFR), a coherent and helical structure in which the magnetic field lines wound around its central axis more than once, is believed to be the underlying magnetic structure of coronal mass ejections (CMEs) as evidenced in lots of white-light observations [44] (see Fig 4). Observationally, the MFR often appears as a twisted hot channel in the Atmospheric Imaging Assembly (AIA) 94 Å and 131 Å passbands [45]. Detailed kinematic analyses by Cheng *et al* have revealed that the hot channel rises earlier and faster than the CME leading front [46]. Thus, the hot channel acts as a driver of the CME formation and eruption in the early phase. Through fitting their kinematical evolution with a function consisting of linear and exponential components, Cheng *et al* further determined the onset of the MFR impulsive acceleration [47]. They suggested that the torus instability might play the important role in initiating the impulsive acceleration of CMEs.

Evidence of MFR existence can also be seen during the eruption of filaments. Li and Zhang studied two failed filament eruptions on 2012 July 29 and August 4 and found that the interaction between the erupting surge and a loop-shaped filament supplied much bright mass to the flux rope body, displaying a helical trajectory [48]. The helical motion has also been observed by NVST. Yang *et al* displayed that the filament, after activated by magnetic field cancellation, rose and flowed along helical threads, tracking the twisted structure of the MFR [49].

Liu *et al* investigated the propagation of an extreme solar storm event with multi-point remote-sensing and *in situ* observations [50]. They found that the in-transit interaction between two closely launched CMEs led to the extreme enhancement of the ejecta magnetic field detected near 1 AU at STEREO-A. The fast transit to STEREO-A or the unusually weak deceleration of the CME was caused by the upstream solar wind by an earlier CME. These results show how an extreme space weather event can arise from the interaction of multiple CME eruptions.

Feng *et al* examined energy partition of the active region AR 11283 that hosted an Earth-directed CME [51]. They have found that the released free magnetic energy is about 6.4×10^{31} erg. The sum of the kinetic and potential energy of the CME may amount to 6.5×10^{31} erg. Therefore, the released magnetic energy seems enough to power the eruption of the CME and the flare emission.

Cheng *et al* investigated the formation of the MFRs [52]. They found that the helical field of an MFR, indicated by the continuous sigmoidal emission feature, was formed from two sheared arcades near the main polarity inversion line. The driver of the reconnection was shearing and converging motions of magnetic footpoints. The non-linear force-free field structures disclosed that the reconnection occurred in a bald-patch region and in a hyperbolic flux tube. Using the IRIS data, Cheng *et al* further uncovered that the Si IV, C II, and Mg II lines displayed redshifts and non-thermal broadening at the footpoints of the MFR [53]. However, at its formation site, there appeared a relatively large blueshift and an extremely strong non-thermal broadening. These spectral features confirm that magnetic reconnection actually plays an important role in the formation of MFRs.

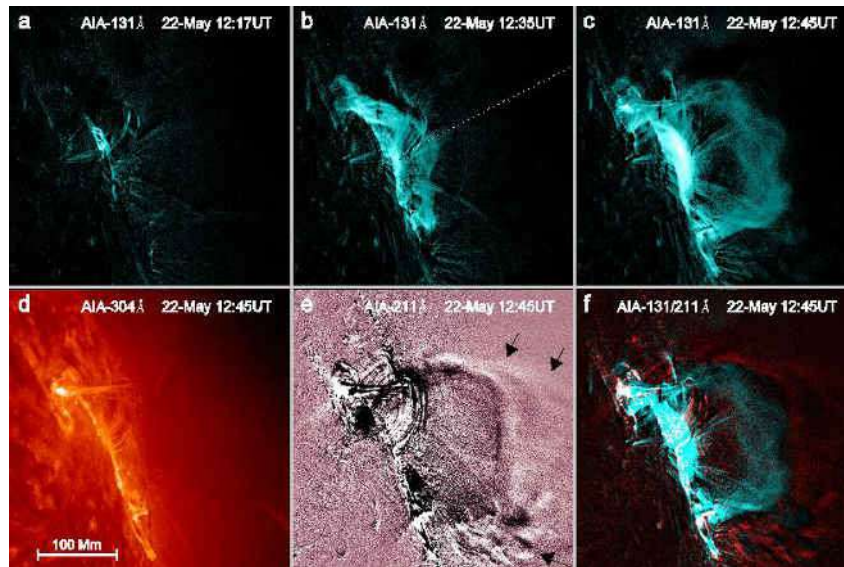


Fig 4. A MFR on 2013 May 22 observed at different wavelength channels by AIA on board SDO [44].

On the other hand, Song *et al* presented an observation of the formation process of the MFR during the eruption [54]. The process began with the expansion of a low-lying coronal loop, which stretched the overlying field and formed an X-shaped structure. The field lines nearby continued to approach each other and then reconnect, leading to the formation and eruption of the MFR. In another event, Chen *et al* investigated two successive solar flares and found that some pre-existing loop structures interacted with each other before the flare, producing a brightening region beneath the filament [55]. At the same time, a small brightening appeared below the interaction region and new helical lines were formed and added into the MFR. This is basically consistent with the tether-cutting picture.

Photospheric magnetic field evolution is an important precursor of solar eruptions. Ruan *et al* studied the pre-flare magnetic field evolution of the X2.1 event from AR 11283 [56]. They found that both the horizontal field strength and the inclination angle (the angle between the vector magnetic field and the local radial direction) declined gradually. Such a change is associated with the overall ascending motion of the filament-flux rope structure. Ruan *et al* investigated another X1.8 flare from the same active region [57]. They found a long-term pre-flare penumbral decay and a transverse field decline, which could be taken as possible precursors of an eruption.

2.2.2 Observations of filaments, flares and jets

Thanks to the rapid development of high-resolution space-borne and ground-based solar telescopes, filaments have attracted an increasing interest. Yan *et al* studied the formation and magnetic evolution of two active-region filaments [58]. They found that the shearing motion of the opposite magnetic polarities and the rotation of the small sunspots played an important role in the formation of filaments. The filaments are not static after formation. Once being disturbed, they would oscillate. Shen *et al* presented the first observation evidence of simultaneous transverse oscillations of a prominence and a filament and longitudinal oscillation of another filament launched by a single shock wave [59]. The orientation of a filament relative to the normal vector of the incoming shock is a key factor that determines the direction of oscillations. Bi *et al* reported the large-amplitude (35–42 Mm) longitudinal oscillations and material drainage in a filament [60]. The filament material drainage is found to be crucial in the transition from a slow to fast rise of the eruptive filament.

Using both imaging and spectroscopic observations, Chen *et al* found that there were two components in the counter-streaming of filaments: longitudinal oscillations of threads and unidirectional flow inside each thread. Most filaments would erupt at their final stages [61]. However, the triggering mechanism of eruption is still unclear. Yan *et al* argued that kink instability is responsible for the triggering of the filament eruption, observed on 2012 May 22 [62]. It is noted that not all filaments were fortunate to escape out of the corona. The filaments in active region 12192 underwent homologous confined eruptions due to the strong stress from the overlying magnetic field [63]. Zhang *et al* observed a partial filament eruption [64]. The filament first split into two parts; then, the major part underwent failed eruption while the runaway part escaped and produced a weak white-light CME. Besides case studies, statistical analyses are also interesting. Hao *et al* developed an advanced automatic method for filament recognition and tracking and applied it to one solar cycle of H α data [65].

According to the standard flare model, filament eruptions are often accompanied by two-ribbon flares. When the accelerated nonthermal electrons impinge on the chromosphere, hard X-ray (HXR) emissions are created via Coulomb collisions, and the local plasmas are heated followed by chromospheric evaporation. Using imaging and spectroscopic observations, Li *et al* found direct evidence of electron-driven evaporation during the impulsive phase of flares [66]. The Doppler velocities are highly correlated with the HXR fluxes at various energy bands. Li *et al* found that gentle and explosive evaporations take place at different locations [67]. There is a conversion from gentle to explosive evaporations. Li *et al* observed quasi-periodic pulsations with a period of ~ 4 min over a wide spectral range from radio to HXRs during the X1.6 flare on 2014 September 10 [43]. The authors conjectured that periodic magnetic reconnections were modulated by a slow-mode wave.

The major peak of a flare may sometimes be followed by a second peak with a lower amplitude in EUV wavelengths, which is termed as the EUV late phase. The time delays between the two peaks range from tens of minutes to several hours. Dai *et al* found that distinct from the main flare loops, the warm EUV late phase loops were produced by the least energetic magnetic reconnection stage [68]. Liu *et al* found that the late phase loops were larger and higher than the main phase loops [69]. They have proposed that the EUV late phases originate from the long-lasting cooling process in the larger magnetic arcade system. Li *et al* investigated the roles of both cooling and additional heating in the production of late phase emission [70].

Coronal jets are also an interesting topic in recent years. The anemone jets are usually associated with a magnetic null point and the fan-spine system. Using the line-of-sight magnetograms and potential field modeling, Zhang *et al* identified two null points in the coronal bright points (CBPs) at the bottom of jets [71]. Similar fan-spine dome with ultrafine structures has been observed by IRIS and SDO [72]. Sometimes, coronal jets show untwisting or rotation motions when the stored magnetic helicity is being transferred. The rotating jets have been observed at the boundaries of active regions [73] and coronal holes [74]. Zhang & Ji observed recurrent plasmoids or blobs in the homologous jets [75]. They studied the sizes and physical parameters of the blobs, such as velocity, temperature, and density. Recently, the connection between a jet and a CME is discovered by Liu *et al*, who found that the jet triggered the CME and became the CME core [76]. Huang *et al* found that a solar surge might be the trigger of the filament eruption and the following-up flare and CME [77]. These results have considerably enriched our understanding of the triggering mechanisms of solar eruptions.

A zebra pattern (ZP) structure is the most intriguing fine structure on the dynamic spectrograph of a solar microwave burst. For the first X-class flare event in the 24th solar cycle on 2011 February 15, several interesting microwave ZPs including an unusual high-frequency ZP structure up to 7.00 GHz that occurred in the early rising phase of the flare were observed by the Chinese Solar Broadband Radio Spectrometer (SBRs/Huairou & SBRs/Yunnan). It is suggested that the double plasma resonance model is the most probable mechanism for explaining the formation of microwave ZPs [78]. A comprehensive statistical analysis of a big sample with 202 ZP events has been carried out by Tan *et al* [79]. It is found that the variation of zebra stripe frequency separation with respect to frequency is the best indicator for a physical classification of ZPs. Microwave ZPs can be classified into three types: equidistant ZPs, variable-distant ZPs, and growing-distant ZPs, possibly corresponding to mechanisms of the Bernstein wave model, whistler wave model, and double plasma resonance model, respectively. This statistical classification may help to clarify the controversies between the existing various theoretical models and understand the physical processes in the source regions.

2.2.3 Magnetic topology and MHD simulations

Fu *et al* applied two different ways to search for the location of magnetic null points [80]. One is the first order Taylor expansion and the other is the Poincare index. The results provided by the two methods are generally consistent, while the former could derive the position of a magnetic null point with higher accuracy than the latter. The former method could also provide the information of the type and the associated topology of the null point. This method is ready to apply to observations.

Yang *et al* studied the magnetic topology associated with a circular ribbon flare with multi-wavelength data provided by SDO, Hinode, and RHESSI [81]. A new algorithm is implemented to compute the 3D magnetic topology with the squashing degree distribution (see Fig 5). The nonlinear force-free field optimization method is adopted to reconstruct the magnetic configuration. Three distinct but closely related magnetic topological structures are found, a magnetic flux rope, a null point, and a large-scale quasi-separatrix layer (QSL). These features could explain the hard X-ray sources at the footpoints of the magnetic flux rope, the evolution of the inner and circular flare ribbons, and the large-scale dome-like and loop-like emission features in AIA 94 Å.

The EUV late phase of flares is found to be related to specific magnetic topologies. Li *et al* studied the magnetic origin of late phase for four different flares [70]. The results show that three of them are caused by the long hot spines associated with magnetic null points. The magnetic field for the other flare also contains a null point, but the late phase is associated to some large-scale magnetic loops. After an analysis of a long duration flare, Liu found that the continuing magnetic reconnection at the QSLs, which are associated with the bald patch of a magnetic flux rope and the hyperbolic flux tube (HFT) of large-scale multi-polar magnetic loops, might account for the prolonged emission of the flare [82].

Through a series of nonlinear force-free field modeling, Jiang *et al* found that a null-point topology is formed after emergence of a bipole into one polarity of preexisting bipolar active region [11]. A bald patch is also formed during the process of magnetic flux rope formation. Driven by the torus instability, the flux rope expands and causes the magnetic reconnection around the null point. The magnetic reconnection could further drive the eruption by removing the magnetic tension force. Zhao *et al* studied the magnetic topology evolution in a flare productive region [83]. They found that a magnetic flux rope associated with a lower lying HFT was located under a higher HFT. The higher HFT was produced by the large-scale magnetic quadrupole. It seemed to only play a second role in the flux rope eruption. A quadrupole magnetic structure could also form a magnetic null point. Sun *et al* found such a magnetic null point above a trans-equatorial active region group. This topology explains an X-shaped EUV structure observed by SDO/AIA [84].

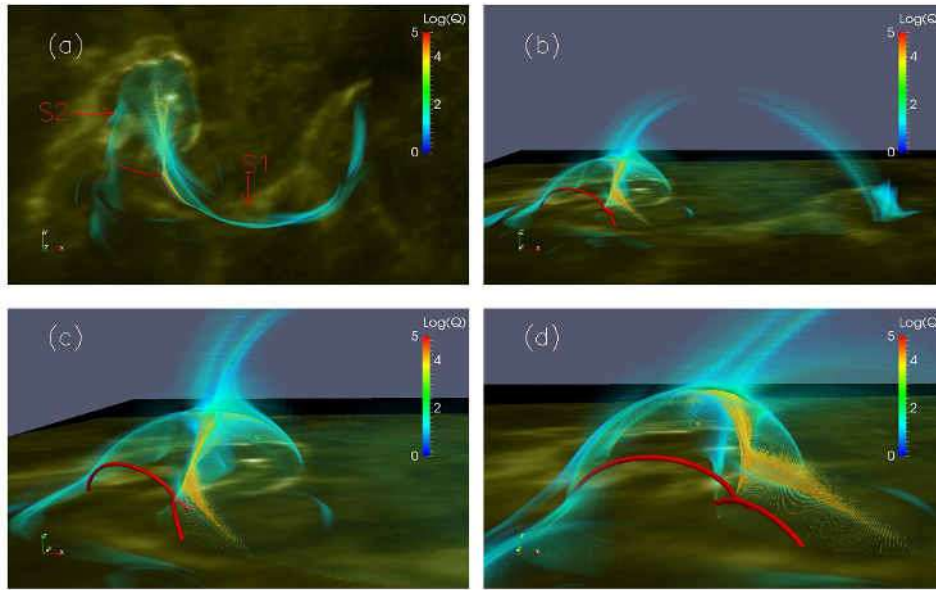


Fig 5. The 3D Q-map showing the QSL structure of the active region 11598 that produced the circular ribbon flare on 2012 October 23 [81].

Guo *et al* compared quantitatively the magnetic helicity injection from the photosphere and the magnetic helicity content in a magnetic flux rope [85]. The magnetic helicity injection is computed by the evolution of the vector magnetic field and the velocity field derived from it; while the magnetic helicity of the flux rope is estimated by its twist and magnetic flux. It is found that only a small fraction of the injected magnetic helicity is stored by the magnetic flux rope itself. The flux rope is wrapped by a QSL, where magnetic reconnection is prone to occur to add magnetic flux to the rope.

Magnetic reconnection is the most important energy release mechanism in the solar atmosphere. Ni *et al* performed a 2.5D MHD simulation to study the fast magnetic reconnection caused by the plasmoid instability [86]. They considered the radiative cooling, heating, and ambipolar diffusion effects. It is found that radiative cooling and ambipolar diffusion could influence the reconnection process when the guide field is not included. Ni *et al* further studied the energy spectrum in a current sheet by a simulation with realistic physical parameters [87]. The energy spectrum along the current sheet is not a power law with a single index. Part of the magnetic energy is converted into a space with large wave numbers.

With a 3D MHD simulation, Jiang *et al* studied the eruption of a magnetic flux rope [14]. The initial condition is provided by the data from an observation, namely, from the nonlinear force-free field model.

They found that the magnetic reconnection in a magnetic null point triggered the eruption, and that the torus instability drove the full eruption of the magnetic flux rope. The numerical simulation well reproduces the eruption process observed by SDO/AIA.

Numerical simulations have also been performed to study the formation, oscillation and eruption of solar prominences. Zhang found that the magnetic null point in the inner corona plays a critical role in solar prominence dynamics [88]. She performed a 2.5D MHD simulation to show that prominences are relatively easy to form and erupt when there is a null point and with large maximum value of the background magnetic field. Zhang *et al* conducted a set of detailed 1D radiative hydrodynamic simulations to study the restoring force and damping mechanisms for the longitudinal prominence oscillations [89]. It is found that the restoring force is mainly provided by the gravity if the prominence is long or by the gas pressure gradient when it is short. The damping is mainly caused by the radiative loss and partly contributed by the thermal conduction.

2.3 Coronal heating and solar wind

Magnetic reconnection and waves/turbulence are believed to play essential roles in heating the corona and accelerating the solar wind, while indirect, spectroscopic diagnostics of loops and small scale dynamic events in the solar atmosphere can offer the crucial information on how these mechanisms work. In interplanetary space, direct *in situ* measurements of the solar wind turbulence yield how turbulence works, which is expected to be operational in the solar corona as well. State-of-the-art analysis yields that kinetic Alfvén waves may be an essential ingredient that comprises turbulence close to kinetic scales.

2.3.1 Physical diagnosis in the solar atmosphere

Since the corona is believed to be occupied by numerous magnetic loops with different heights or funnels open into interplanetary space, the coronal heating processes are often considered as heating the coronal loops and funnels in the solar atmosphere. Besides, the magnetic funnels are generally accepted as channels, in which the solar wind is accelerated and flows out. On the other hand, small scale dynamic events, such as coronal bright points, jet-like events, nanoflares, transition region explosive events, etc., are believed to play an important role in understanding the coronal heating problem.

Impulsive and steady heating processes are two major mechanisms that heat the solar corona to above a million degrees. Which mechanism is at work depends on the physical conditions of the coronal structure where the heating is taking place. Li *et al* found that the evolution and dynamics of the two sets of flaring loops were quite different, which might suggest different heating mechanisms [90]. In order to test the validity of the nanoflare process, Li *et al* found that a fast heating of a hot loop was followed by about an hour of cooling process, and the comparison to the predictions from a 1D loop model showed that this observation appeared to support the nanoflare process [91]. Li *et al* concluded that the nanoflare-heating scenario better explains ultraviolet loops, while turbulence-based steady heating mechanisms might be at work in heating a fraction of soft X-ray loops [92].

In the past, observation and numerical analysis are mostly concentrated on hot and warm loops because the cooler loops are more dynamic and difficult to be observed. The launch of the IRIS mission has provided an opportunity to investigate the cool transition region loops. Huang *et al* reported on the first IRIS study of cool transition region loops [93]. They found that cool transition region loops were very dynamic, fine-structured and diverse. With the spectral data, they also discovered evidence of siphon flow and magnetic reconnection in the loops in agreement with the impulsive heating process.

Considering that the solar magnetic field is spatially inhomogeneous with a considerable magnetic gradient from the solar surface to the corona, recently, Tan proposed a magnetic gradient pumping (MGP) mechanism to explain the formation of hot plasma upflows, such as hot type II spicules and hot plasma ejections [79]. In the MGP mechanism, the magnetic gradient may drive the energetic particles to move

upward from the underlying solar atmosphere and form hot upflows. These upflow energetic particles are deposited in the corona, causing it to become very hot. Rough estimations indicate that the solar corona can be heated to above 1 million degrees, and the upflow velocity is about 40 km s^{-1} in the chromosphere and about 130 km s^{-1} in the corona. The solar magnetic flux tubes act as pumpers to extract energetic particles from the underlying thermal photosphere, convey them, and deposit them in the corona. The deposit of these energetic particles causes the corona to become hot, and the escape of such particles from the photosphere leaves it a bit cold. This mechanism can present a natural explanation to the mystery of solar coronal heating.

Coronal bright points (BPs) are small-scale bright patches embedded in the solar corona where local heating is taking place. BPs have been intensively studied since they were first discovered in 1970s, and some new knowledge has been topped-up into this field in the recent years. BPs might be heated by magnetic reconnection [94], which is also supported by their connection with magnetic cancellation [95]. Zhang and Ji observed chromospheric evaporation in sympathetic coronal bright points, which is also evidence of magnetic reconnection [96]. A large number of BPs are associated with mini-filament eruption [97], and moving bright structures [98], which are evidence of magnetic reconnection taking place in BPs.

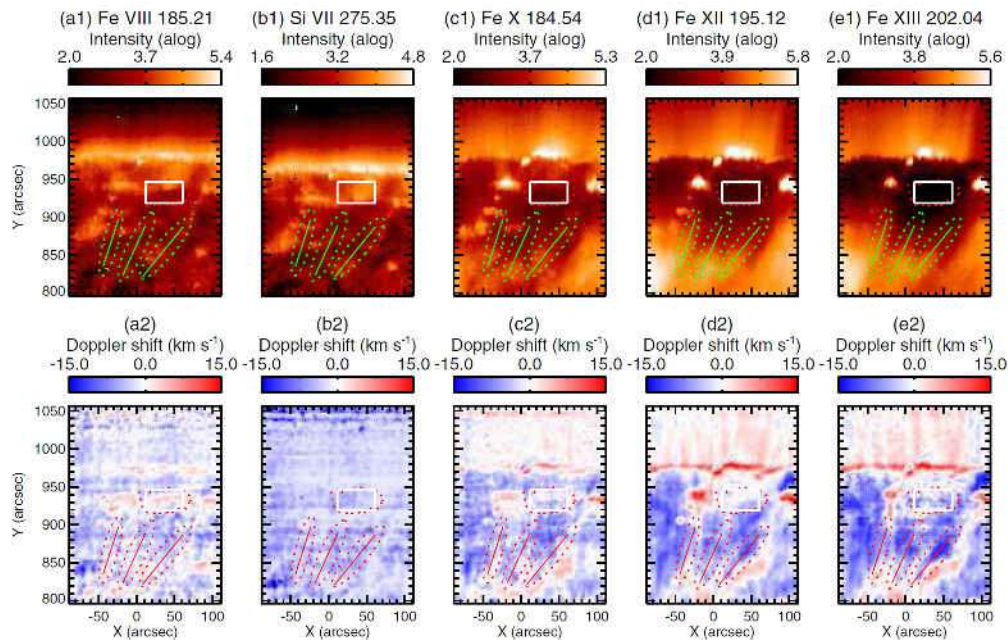


Fig 6. Intensity map and Dopplergram as recorded by EIS/Hinode in the Fe VIII 185.21 Å, Si VII 275.35 Å, Fe X 184.54 Å, Fe XII 195.12 Å, and Fe XIII 202.04 Å lines on 2007 October 10. The plume structures (indicated by three tilted lines) are clear in Fe XII 195.12 Å and Fe XIII 202.04 Å and coincide with strong blueshift patches derived from these two lines [103].

Transition region explosive events are characterized by their non-Gaussian spectral profiles, which are suggested to be signatures of magnetic reconnection in the low solar atmosphere that might take part in the coronal heating process. Huang *et al* observed an explosive event that occurred in a complex small-scale loop system and was heated to mid-transition-region temperature, and they suggest that the explosive event is result of magnetic reconnection between the loops [99]. The loop reconnection scenario is also supported by high-resolution observations of transition region loops by IRIS [93]. Non-Gaussian spectra with self-absorption phenomena in the transition region observed by the IRIS suggest complexity in the solar atmosphere with magnetic reconnection occurring everywhere [100].

Large-scale quiet-Sun (QS) can be heated by the interaction between emerging active region (EAR) and their surrounding QS [101]. They found that ribbons visible in EUV wavelengths appear at the boundary of the EARs and the QS, and propagate away from the EARs with speeds of a few km s^{-1} . Moreover, the regions swept by the dark ribbons are brightening afterward, with the mean temperature increasing by one quarter. These observational discoveries demonstrate that uninterrupted magnetic reconnection between EARs and the QS occurs.

The origin of the solar wind is another key problem. Recent spectroscopic observations with SUMER/SOHO suggested a new scenario for the origin of the solar wind, in which the nascent wind flows out in a magnetically open coronal funnel and the mass flux is supplied to the funnel by means of reconnection between the magnetic funnel and small-scale side loops. To validate this model, magnetic reconnection driven by supergranular convection has been numerically simulated [102]. Their study demonstrates that the mass flux of the outflow released from the funnel is appropriate for providing the mass flux at the coronal base of the solar wind.

The contribution of plumes to the solar wind has been subject to hot debate in the past decades. The EUV Imaging Spectrometer (EIS) on board Hinode provides a unique means to deduce outflow velocities at coronal heights via direct Doppler shift measurements of coronal emission lines. Fu *et al* measured the outflow velocity at coronal heights in several on-disk long-duration plumes in coronal holes (CHs) and show significant blueshifts throughout the entire observational period (see Fig 6) [103]. The results indicate that CH plumes may be an important source of the solar wind.

2.3.2 Waves and oscillations

Considerable progress has been made in the studies on waves and oscillations in the solar atmosphere since the late 1990s, thanks to the availability of high tempo-spatial resolution data from both ground- and space-based instruments. On the one hand, waves may play an important role in sustaining the solar corona at multi-million degrees Kelvin. On the other hand, their measurements can help yield atmospheric parameters that are difficult to measure directly, the coronal magnetic field strength in particular.

Propagating intensity disturbances (PDs) in polar coronal holes, with intensity variations of a few percent relative to the background, have been of considerable interest since the 1980s. Despite this long history, the nature of PDs remains debated. While slow magnetoacoustic waves seem a natural interpretation given that PDs propagate at roughly the sound speed, there is also evidence suggesting that PDs may be quasi-periodic upflows. The wave scenario was corroborated by a recent study on the phase speeds of PDs as measured with image sequences obtained by SDO/AIA in its multi-passbands [104]. The speed ratios in different passbands were found to be consistent with the theoretical expectations for slow waves. However, also using AIA data, Jiao *et al* showed that PDs in the corona tend to be correlated with spicular activities in the lower atmosphere, meaning that upflows impinging on the transition region or coronal base can be a source for PDs [105]. This suggests that the upflow and wave scenarios are not necessarily mutually exclusive, and points to the possibility that not all frequency components in the power of PDs need to be contrasted with theoretical expectations for slow waves.

Quasi-periodic fast waves with multiple arc-shaped wavefronts had not been seen before the SDO era. Continuously emanating from flare kernels and propagating at speeds $\sim 1000 \text{ km/s}$, these wave trains are suggested to be fast magnetosonic waves generated by flares. Their fast wave nature was illustrated by a recent observational study using multi-passband AIA data where wave trains were shown to decelerate in response to variations in magnetic and plasma parameters of the guiding inhomogeneity [106]. The same study also attributed the periodicity shared by both wave trains and the source flare to periodic energy releases during magnetic reconnection (MR). This interpretation was supported by a numerical study by Yang *et al* [107], who showed that MR can tear current sheets into plasmoids, which then collide with the ambient magnetic field when reaching the outflow regions, thereby generating fast wave trains in a consecutive manner.

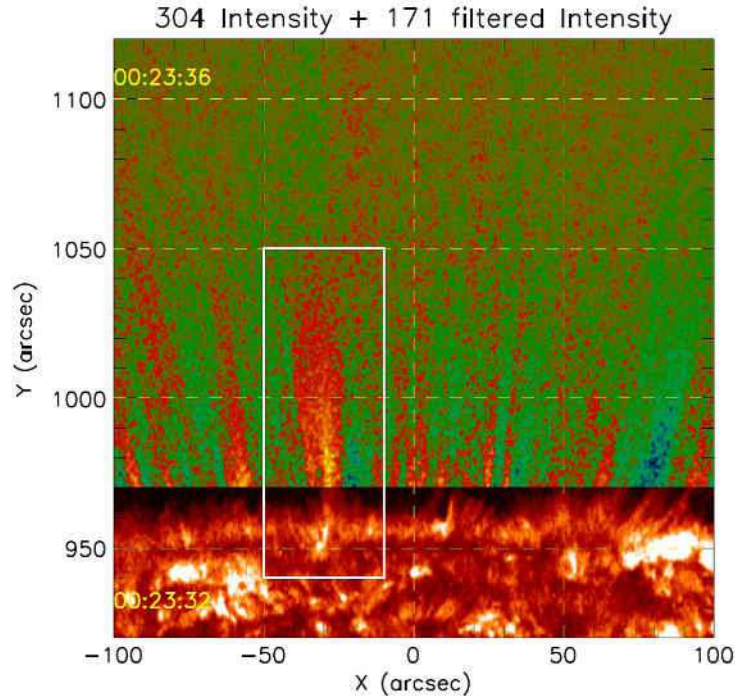


Fig 7. Composite image constructed from the original AIA 304 Å (bottom) and filtered AIA 171 Å (top) images shows the correlation between the spicular activities and the PDs. Spicules are visible in the AIA 304 Å image, while PDs are clear in the filtered AIA 171 Å images [105].

AIA data have also shed new light on the long standing discrepancy between the propagation speeds of Moreton waves in the chromosphere and coronal EUV disturbances originally named EIT waves [108]. The authors suggested that wave fronts ahead of a typical EIT wave were the coronal counterpart of Moreton waves. While the faster component seems unmistakably to be fast magnetosonic waves, it remains debated as to whether the slower components are real waves. The resolution of this issue may benefit from observational studies on the interactions between this slower component and various features like filaments [109], active regions and coronal holes [110].

Quasi-periodic pulsations (QPPs) in the lightcurves of solar flares were recognized in the late 1960s. Although early studies were largely restricted to microwave emissions, multi-wavelength studies have become increasingly popular. For instance, Huang *et al* showed that oscillations with periods $\sim 20\text{--}30$ s in microwave, EUV and Soft X-Ray emissions are in phase for the event examined therein, and attributed these oscillations to fast kink modes [111]. In another multi-instrument, multi-wavelength study, Li *et al* indicated that QPPs in different wavelengths tend to have different periodicities, even though they had a 4-minute one in common [112]. The authors interpreted the QPPs in terms of quasi-periodic magnetic reconnections. These studies suggest that QPPs with periods longer than a couple of tens of seconds may need to be examined on a case-by-case basis.

QPPs with periods of the order of seconds are usually interpreted in terms of standing fast sausage modes in flare loops. The measured periods and damping times can therefore be used to deduce the transverse Alfvén time and density distribution transverse to flare loops. While previous attempts largely relied on idealizing the transverse density profile as a step-function one, Chen *et al* addressed the uncertainties with

the deduced parameters by accounting for more realistic continuous density profiles of arbitrary form [113]. The authors showed that when only one mode is identifiable in the oscillating signals, the density length scale is difficult to constrain given the uncertainties in prescribing the density profiles. However, the situation improves substantially if spatially resolved QPPs involve more than just one sausage mode. This was illustrated in Guo *et al* who examined a QPP event where a temporally decaying kink mode was suggested to co-exist with a sausage one [114]. Attributing the damping of the kink (sausage) mode to resonant absorption (lateral leakage), the authors showed that flare loop parameters, the internal Alfvén speed in particular, are well constrained, even if the specific form of the transverse density distribution remains unknown. Quasi-periodic wiggles of microwave ZP structures with periods ranging from about 0.5 s to 1.5 s were found in an X-class solar flare on 2006 December 13 at the 2.6-3.8 GHz with the Chinese Solar Broadband Radio Spectrometer (SBR/S/Huairou). It is suggested that the ZP wiggles can be associated with the fast magnetoacoustic oscillations in the flaring active region. The lack of a significant phase shift between wiggles of different stripes suggests that the ZP wiggles are caused by a standing sausage oscillation [115].

For seismological purposes, multi-mode oscillations need not to be of different nature. For instance, Guo *et al* employed SDO/AIA data to identify the first two harmonics of horizontally polarized kink modes in a coronal loop system [116]. Besides the inference of the magnetic field strength of the loops, the multi-mode measurements also allowed to examine the effects on the period ratio and eigen-functions of variations in density, temperature and magnetic field strength along the pertinent loop. For the particular event examined therein, structuring in density and temperature was found to play a more important role in determining the period ratio than magnetic field variation.

2.3.3 Kinetic Alfvén waves in the corona and solar wind

Alfvén waves that are permeating the solar atmosphere and solar wind are thought to play an important role in local particle energization. Because the solar atmosphere and solar wind are almost collisionless plasmas, the large-scale Alfvén wave is hard to dissipate through the collision damping. However, the kinetic Alfvén wave can suffer the dissipation due to the Landau resonance mechanism. Therefore, kinetic Alfvén waves are believed to be one of the significant mechanisms contributing to the coronal heating and solar wind acceleration.

A large amount of non-thermal particles are ejected outward from solar flares. These energetic particles can excite directly the kinetic Alfvén wave. Chen *et al* studied the excitation of the kinetic Alfvén wave by the current that is formed by the drift electrons after solar flares, and found that the growth rate was depending on the electron drift velocity and the plasma beta [117]. Using the typical plasma parameters in the flare loops, they found the short relaxation time is 0.01-1 ms. Chen *et al* further studied the impact of the return current corresponding to the electron beam on the kinetic Alfvén wave excitation, and summarized its excitation condition [118].

The solar coronal plasmas are free to move along solar magnetic field lines, but hard to cross transversely the field lines. This anisotropic motion of particles results in the formation of density striation structures in the solar corona, e.g., the bright loops and dark filaments. Wu and Chen studied the excitation of kinetic Alfvén waves by the density striation, and found that the maximal growth rate arises as the wave perpendicular scale is close to the spatial scale of the density gradient [119].

The solar flares can also excite the large-scale Alfvén waves that will propagate along the magnetic field lines in flare loops. When the waves reach the transition region, some fraction of them will be reflected. Therefore, the nonlinear interaction occurs for counter-propagating Alfvén waves. Zhao *et al* studied the Alfvén wave turbulence and turbulent parallel electric field through the nonlinear interaction among Alfvén waves in the flare loops, and explored that the kinetic Alfvén wave is excited as the turbulence cascades into the kinetic scales [120]. They also found that the turbulent parallel electric field at kinetic scales is much

larger than the local Dreicer field, indicating that the effective acceleration of electrons can result from the turbulent parallel electric field in the flare loops. Interestingly, Liu *et al* offered observational evidence with CoMP data that the onset of Alfvénic turbulence can indeed occur in coronal loops due to nonlinear interactions between counter-propagating waves [121].

It is well-known that large-scale finite-amplitude Alfvén waves are widespread in the solar wind. Zhao *et al* considered the nonlinear effects of these finite-amplitude Alfvén waves, and found the strong nonlinear coupling of large-scale Alfvén waves with kinetic-scale Alfvén waves [122, 123]. The nonlinear decay of large-scale Alfvén waves can produce kinetic Alfvén waves, where the wave energy transports directly from the large scale into kinetic scale. Moreover, He *et al* studied the radial evolution of wave vector anisotropy in the solar wind turbulence, and found that the ion-scale turbulence generates predominantly kinetic Alfvén waves at the radial distance larger than 1 AU [124].

He *et al* analyzed simultaneously the wave fluctuations and particle kinetics near the dissipation range in the solar wind turbulence [125]. They discerned the kinetic Alfvén wave mode and drift anisotropic beam in proton velocity distribution, and found the velocity of drift proton beam is of the order of the Alfvén speed. Combining the pieces of observational evidence, they demonstrated the existence of the Landau resonance of kinetic Alfvén waves in the solar wind [125]. He *et al* further observed the sunward propagating Alfvén waves in association with sunward drifting proton beams in the solar wind, and identified again the acceleration of protons by the Landau resonance of kinetic Alfvén waves [126].

2.3.4 Solar wind turbulence

The energy cascade and dissipation processes in the solar wind turbulence are considered to be the major source of coronal and solar wind heating. Small-scale intermittent structures locate at the high frequency end of the inertial range and are very close to the dissipation range. Thus, the small-scale intermittent structures play a vital role in the solar wind energy cascade and dissipation processes.

In the solar wind turbulence, it has been found that the small scales of the turbulence are more intermittent than the large scales. However, the nature of the small-scale intermittency in the solar wind has not been studied observationally. Wang *et al* studied about twenty thousand of magnetic field intermittent structures with the time scale of 24s in details, and found that $\sim 1.8\%$ of them were tangential discontinuity-type (TD-type) intermittency and $\sim 86.5\%$ of them were rotational discontinuity-type (RD-type) intermittency [127]. Moreover, the dissipation mechanism of the solar wind at small scales still remains unknown. To solve this issue, Wang *et al* studied the temperature enhancement of the small-scale magnetic field intermittent structures in the high-speed solar wind [127]. The observational results indicate that the solar wind turbulence dissipation could happen at the TD-type intermittent regions. Conversely, the RD-type intermittency does not show the enhanced temperature. However, because of the small amount of the TD-type intermittency, its contribution to the global heating of solar wind is negligible.

Wang *et al* found that the magnetic reconnection region shows unique multifractal scaling in the dissipation range, while the ambient solar wind turbulence reveals a monofractal dissipation process for most of the time [128]. This result provides the first observational evidence for intermittent multifractal dissipation region scaling around a magnetic reconnection site, and it also has significant implications for the fundamental energy dissipation process.

The phenomenon that the energy spectrum changes with respect to the direction of the local background magnetic field is called the spectral anisotropy. This phenomenon was considered to be consistent with the presence of the “critical balance” type cascade in the solar wind. However, Wang *et al* showed that the observed spectral anisotropy in the inertial range could be caused by the turbulence intermittency other than the “critical balance” cascade [129]. Wang *et al* presented further studies and suggested that the spectral

anisotropy in the inertial range of the solar wind turbulence is the result of the small-scale intermittency [130, 131].

2.4 Solar activity monitoring and forecasting

The magnetic activities and eruptive phenomena in solar atmosphere such as flares and CMEs are the sources of disturbances and variations of space weather in the solar-terrestrial domain as well as the whole solar system. The space weather services in the Chinese solar physics community contain two main portions: solar activity monitoring and forecasting. These services fully rely on the development of solar observations and solar activity forecast modeling. Domestic and international customers of these services are widely distributed in fields of aerospace, communication, navigation, power grid and so on.

2.4.1 Solar activity monitoring

(1) Time-honored Solar Observing Bases

There are three time-honored solar observing bases in China, which are located in Beijing, Kunming (of Yunnan Province), and Nanjing (of Jiangsu Province), respectively. The Huairou solar observing station (HSOS) in Beijing belongs to the National Astronomical Observatories of Chinese Academy of Sciences (NAOC), which can obtain vector magnetogram of solar photosphere, $H\alpha$ image of chromosphere, and solar radio flux and dynamic spectrum. The Yunnan Observatories (YNAO) in Kunming can also provide $H\alpha$ and solar radio observational data. In Nanjing, the solar observations are conducted by the Purple Mountain Observatory (PMO) and Nanjing University (NJU).

(2) New solar observing stations

In recent years, several new solar observing stations were established in China and certain new solar observing devices were put into operation. The New Vacuum Solar Telescope (NVST) at Fuxian Solar Observatory in Yunnan Province can obtain high resolution imaging and spectral data of the solar photosphere and chromosphere. The Ming'antu Ultrawide Spectral Radioheliograph (MUSR) in Inner Mongolia of China can acquire solar radioheliographs in the cm- and dm-wavelength range. NVST and MUSR are operated by YNAO and NAOC, respectively. The Optical and Near-infrared Solar Eruption Tracer (ONSET), a multi-wavelength solar telescope constructed by NJU, is also located at the Fuxian Lake observing station and is jointly operated by NJU and YNAO. Beside these major solar observing instruments, a few of new solar telescopes (observing sunspots, $H\alpha$, and photospheric magnetic field, etc.) were also constructed and operated by other Chinese institutes related to space weather discipline, such as the National Space Science Center (NSSC) of Chinese Academy of Sciences, the National Observatory for Space Weather (NOSW) of China Meteorological Administration, and Shandong University (SDU).

2.4.2 Solar activity forecasting

(1) Operational services

The operational services include short-term (within 3 days), medium-term (timescale of solar rotation), and long-term (time scale of solar cycle) forecasts. Traditionally, NAOC, YNAO, and PMO work together to produce and distribute the medium-term solar activity prediction, while NAOC is responsible for the routine service of short-term prediction. The long-term predictions of solar cycle are published through research papers by the professionals in the Chinese solar physics community. There have been some papers on the prediction of the 25th solar cycle published in several journals [132-135]. The space weather services from NSSC and NOSW produce regularly the forecasts of solar activity [136].

(2) Products of solar activity forecasting

The products of the short-term prediction at NAOC include: (1) solar X-ray flare classes within 2 days (options: none, C-, M-, X-Class); (2) daily solar 10.7 cm radio flux values within 3 days; (3) solar

proton event daily probabilities within 3 days. The products of the medium-term prediction include: (1) monthly mean sunspot number; (2) solar X-ray flare activity level. The product of the long-term prediction is the variation of sunspot number of the coming solar cycle. Currently, the short-term forecasts at NAOC are routinely distributed (via web page and email) every weekday, and the medium-term forecasts (one forecast per week) are distributed every Monday. The long-term forecasts for a coming solar cycle are presented in websites or research papers, which are frequently renewed by authors.

2.4.3 Development of forecasting models

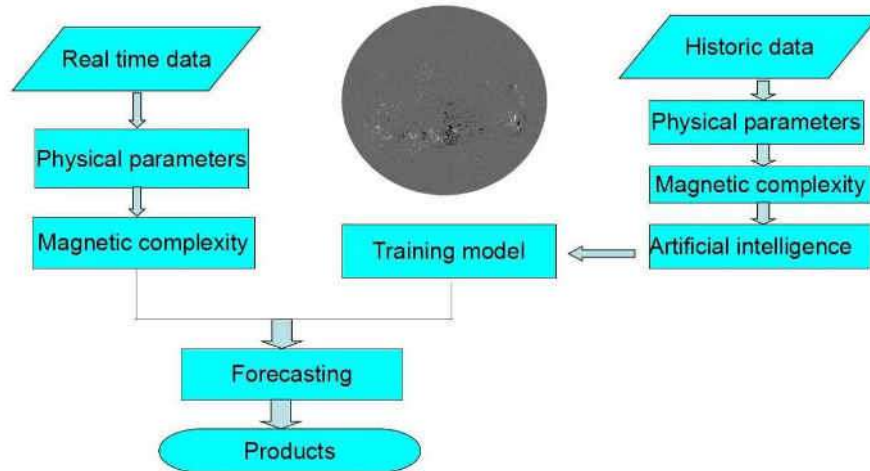


Fig 8. A flow chart of solar flare forecasting model supported with artificial intelligence technique.

Several prediction models of solar activity have been developed and put into operational running at NAOC. For the three short-term prediction products, there are the solar flare prediction model, the 10.7 cm radio flux prediction model, and the proton event prediction model, respectively. The solar active level model and the active longitude model were developed to aid medium-term forecasts. A preliminary CME prediction model was also established at NAOC. It is needed to note that the models are always in revision to incorporate the new research achievements by the whole solar physics community. For example, the latest version of solar flare prediction model is based on the time series of vector magnetic field data obtained by the SDO satellite [137-139]. Recently, the concept of the numerical prediction models for flare and CME predictions is proposed and being realized by the model researchers, which is based on the analyses of the 3D coronal magnetic field configuration and the associated quantitative physical measures of solar photosphere, chromosphere, and corona [140-142]. It is expected that in the future, with the assistant of the artificial intelligence technique, the numerical prediction models will achieve high correct-prediction rate and fully automatic running, and finally release the burden on the human forecasters. In addition, activities of solar-type stars are also analyzed to understand the long-term behaviors of the Sun [143].

2.4.4 International cooperation on operational space weather predictions

The international cooperation on the operational space weather predictions is organized by the International Space Environment Service (ISES). As a member of ISES, Regional Warning Center of China (RWC-China) was established in early 1990s. AS one of the sub-centers of RWC-China, Solar Activity Prediction Center (SAPC) is located at NAOC. NAOC is also the headquarters of RWC-China and is responsible for the daily forecasts and observational data interchange with other Regional Warning Centers (RWCs) around the world. To serve the Asia-Oceania space weather community, the Asia Oceania Space

Weather Alliance (AOSWA) was founded in early 2010s. The space weather professionals in the Chinese solar physics community joined AOSWA from the beginning of its establishment. According to the living evaluations given by RWC-Japan, the solar flare forecast accuracy of RWC-China is at the same level with other leading space weather institutions around the world.



Fig 9. Consultation room for solar activity forecasting at NAOC.

3 Advances in the key project

3.1 New Vacuum Solar Telescope (NVST)

NVST is a vacuum solar telescope with a 985 mm clear aperture [144]. It is the primary optical facility of the Chinese solar community, not only for solar physics but also for space weather enterprise. The first-light of NVST was obtained at Fuxian Solar Observatory (FSO) on September 1st, 2010. The regular operation started from 2012.

3.1.1 Telescope and instruments

The location of FSO is N 24°34' 48" and E102°57' 01", the northeastern side of the Fuxian Lake (Fig 10), with an altitude of 1720 meters above the sea level. The average seeing (Fried parameter, r_0) at FSO obtained in the period from 1998 to 2000 is about 10 cm. The sunshine duration of FSO is about 2200 hours per year [145, 146]. The scientific goals of NVST is to observe the Sun with very high spatial and spectral resolutions in the wavelength range from 0.3 to 2.5 micron; detecting fine scale structure and process in the evolution of the solar magnetic field and their coupling to the plasma in detail; investigating the energy transfer, storage and release in the solar atmosphere, such as the issues of corona heating, the triggering of the solar eruption, and the other key questions regarding solar activities.

NVST is designed as a vacuum telescope in order to reduce turbulence in the system. An optical window with a diameter of 1.2 meters is placed on the top of the vacuum tube to keep the air pressure inside the tube lower than 70 Pa. The optical system after vacuum window is a modified Gregorian system with an effective focal length of 45 m. The mounting system of NVST is an alt-azimuth structure. The telescope is installed on the top-front part of a building that is 16 meters high. The roof of the building is designed to have a shallow pool filled with water that produces a cooling effect against sunshine heating. With a moveable dome, in most cases, the telescope works in open air in order to maintain good local seeing. An active louvered windscreen fences the telescope against wind and guides wind toward the floor, reducing turbulence near the ground.



Fig 10. Building (left), telescope and the wind screen (right) beside Fuxian Lake.

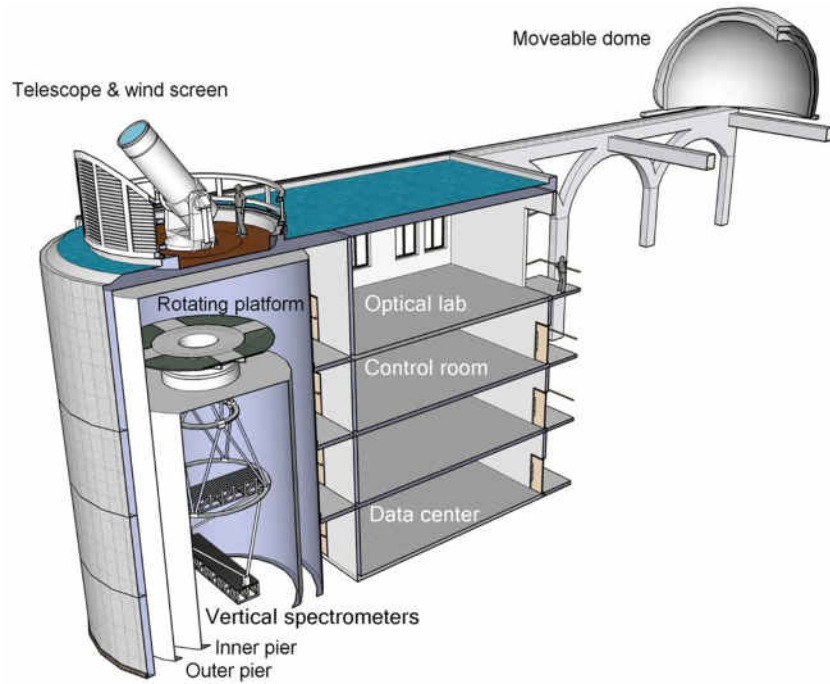


Fig 11. A 3D sketch of the whole building.

The instruments that are utilized by NVST are designed for performing observations related to the scientific goals. They are located either on the rotating instrument platform or on the frames of the vertical hanging bracket below the telescope (Fig 11). These instruments basically consist of three groups according to their functions and working modes. The first group includes the 151-elements adaptive optics (AO) system and a polarization analyzer (PA). The PA is placed before the slit of the spectrometer but the calibration unit is installed close to second Gregorian focus, making it located in a symmetrical optical system. Combining with the spectrometers, the polarization system can conduct measurements of the Stokes parameters at 5324

and 10830 Å. The second group consists of all imaging instruments mounted on the rotating platform. Its main structure is a 5-channel high resolution imaging system. The bands for observing the chromosphere are H α (6563 Å), Ca II (3933 & 3968 or 8542 Å) and He I (10830 Å). The bands for observing the photosphere are TiO (7058 Å) and G-band (4300 Å). The third group includes two vertical grating spectrometers placed in the hanging bracket below the rotating platform. The spectrum resolution of the Multi-Band Spectrometer (MBS) [147] is about 100,000 and mainly works in the visible range, e.g. Fe I (5324 Å), H α and Ca II (8542 Å). The High Dispersion Spectrometer (HDS) is a near infrared spectrometer with a spectrum resolution up to 400,000 at 1.56 micron. A magnetograph with high spatial resolution has also been designed in order to match the resolving power of the current multi-channel imaging system.

3.1.2 The high resolution observations made by NVST

High resolution observation of active regions (Fig 12) is the primary science task of NVST during the 24th solar cycle. There are more than 600 TB raw data have been recorded by NVST from 2012. The data output from NVST is classified into two levels. The level-1 data are processed by frame selection. The level-1+ data are reconstructed by speckle masking [148] or iterative shift and add [149]. After reconstructed by speckle techniques, the spatial resolution of an image of the photosphere (G-band) could reach nearly 0.1" in good seeing conditions, and the spatial resolution of an image of the chromosphere (H α) is better than 0.2". The observational data acquired at NVST, including images and movies, are now available on line (<http://fso.ynao.ac.cn>).

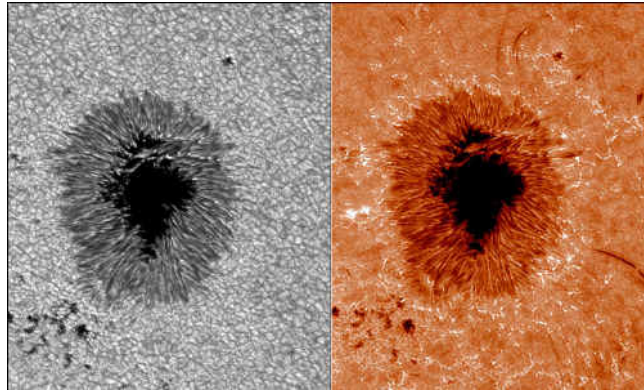


Fig 12. High resolution reconstructed images of the photosphere (7058 Å, left) and the chromosphere (H α -0.8 Å, right) showing a sunspot in the active region NOAA 11598.

Researches based on these data are mainly focus on the fine structures and their evolutions in solar atmosphere, such as the small-scale reconnection, details of active region and fine structures of prominence (filament). Yang *et al* presented observational indications of magnetic reconnection that occurs between two sets of small-scale, anti-parallel loops [39]. One of the interesting phenomena in this high-resolution observation is the clear but very slim current sheet. Yan *et al* observed the evolution of NOAA 11884 and found that the shearing motion of the opposite magnetic polarities and the rotation of a small sunspot play an important role in the formation of two active-region filaments [58]. Shen *et al* observed fine structure of a quiescent prominence and analyzed the collapsing of a bubble structure inside it [150] (Fig 13). This set of observations demonstrates the superior seeing condition at the site of Fuxian Lake.

These above high-resolution observations and the relevant investigations show the typical function of a modern big aperture solar telescope. Considering that it is located between Europe and America, NVST could work in combination with other large solar telescopes to form a global high-resolution observation network.

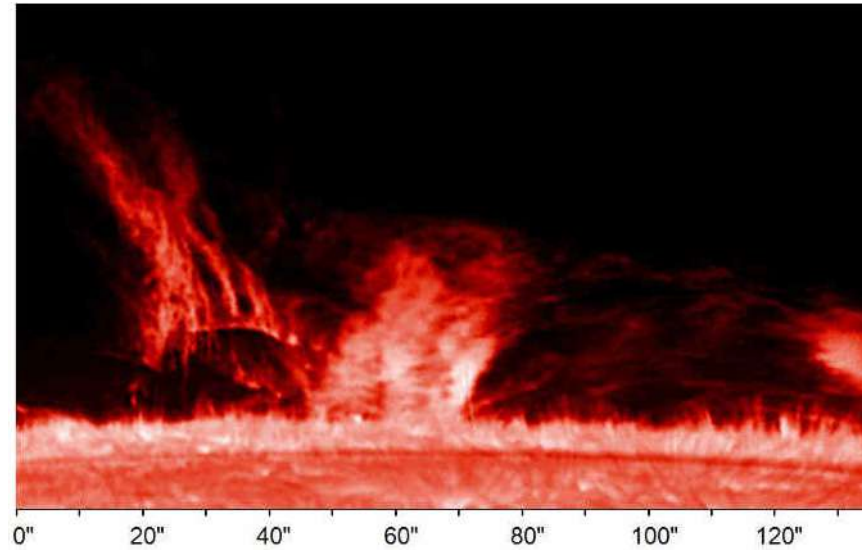


Fig 13. High-resolution observation of a quiescent prominence.

3.2 Ming'antu Ultrawide Spectral Radioheliograph (MUSER)

3.2.1 Motivation

Radio bursts are prompt indicators of the various solar activities including flares and CMEs, etc. RHESSI observations indicate that non-thermal particles may account for a significant fraction of flare energy released during the impulsive phase. Imaging spectroscopy over centimeter and decimeter wavelengths is important for addressing the problems of primary energy release, particle acceleration, and transportation processes.

From statistical study of radio dynamic spectral observations it has been inferred that the acceleration site is located in a low-density region with an electron density of $\sim 3 \times 10^9 \text{ cm}^{-3}$, corresponding to a plasma frequency of 500 MHz, from where electron beams are accelerated in upward (type III) and downward (RS bursts) directions. However, the available radio imaging observations are presently only at a few discrete frequencies in the range 40–150 MHz from Gauribidanur Radioheliograph, in the range 150–450 MHz from Nancay Radioheliograph, at 5.7 GHz from Siberian Solar Radio Telescope, and at 17/34 GHz from Nobeyama Radioheliograph [151].

Therefore, it is expected to have a new instrument that is capable of true imaging spectroscopy, with high temporal, spatial, and spectral resolution. The Chinese Spectral Radioheliograph (CSRH) has been proposed to reach this goal, which will open new observational windows on flares and CMEs at radio wavelengths.

CSRH has been supported as the National Major Scientific Research Facility Program of China. The whole budget for CSRH project was approved in 2009. The site survey for the CSRH array was completed at Ming'antu town in Inner Mongolia of China and the radio quiet zone protection with 10 km radius centered at CSRH site was setup in 2008. The construction also started in the autumn of 2008. The whole CSRH system is finished by the end of 2013 and is in commission observations now. CSRH is renamed as Ming'antu Ultrawide Spectral Radioheliograph (MUSER) after its accomplishment. Figure 14 shows the MUSER array.



Fig 14. Central part of MUSER array.

3.2.2 Description of MUSER

MUSER in centimetric/decimetric wave range is a solar-dedicated radio interferometric array that will be used to carry out imaging spectroscopy of the Sun, to produce high spatial resolution, high time resolution and high frequency resolution images of the Sun simultaneously. The updated main specifications of MUSER are listed in Table 1.

Table 1. MUSER specifications

Frequency range	0.4-15 GHz (λ : 75-2 cm)
Frequency resolution	64 channels for MUSER-I (0.4-2 GHz) 520 channels for MUSER-II (2-15 GHz)
Spatial resolution:	MUSER-I: $\sim 10''$ - $50''$ MUSER-II: $\sim 1.3''$ - $10''$
Temporal resolution:	MUSER-I: ~ 25 ms MUSER-II: ~ 200 ms
Dynamic range	25 db (snapshot)
Polarizations	Dual circular L, R
Array	MUSER-I: 40 \times 4.5 m parabolic antennas MUSER-II: 60 \times 2 m parabolic antennas
Maximum baseline	3 km
Single dish beam (Field of view)	~ 0.6 - 7 deg

The MUSER's frequency range is divided into MUSER-I covering 0.4-2GHz and MUSER-II covering 2-15 GHz. The MUSER-I contains 40 antennas of 4.5 m diameter, and the MUSER-II contains 60 antennas of 2 m diameter. The whole 100 antennas of whole MUSER array form 3 log-spiral arms, and the maximum baseline length is 3 km. An additional two 20 m antennas for interferometry experiment in 400-1000 MHz were established in 2011 in MUSER site, which can be incorporated for MUSER-I calibrations later. The solar radio emission in 0.4-2 GHz is received by each MUSER-I antenna with the broadband feed and outdoor devices including LNA and optic transmitter. The signal with 400 MHz bandwidth, which

covers the whole 1.6 GHz bandwidth by scanning 4 times, is then transmitted through optic fibers to indoor devices including optic receiver and analogous receivers with an output in 50-450 MHz range. It is then followed by digital receiver with 1 Gbps A/D converter to receive 400 MHz analogous signal and the digital receiver outputs 16 channels simultaneously for the complex correlations with 2-25 MHz bandwidth for each channel. The time delay compensation and fringe stopping are considered in the digital correlations. The whole correlation procedure is controlled by a monitoring subsystem. Similar procedure applies to MUSER-II except that the solar radio emission in 2-15 GHz is received by each MUSER-II antenna with the broadband feed and the IF signal with 400 MHz bandwidth will need to scan the whole 13 GHz bandwidth by 33 times now.

3.2.3 Status of MUSER

Among aperture synthesis technique based technical issues for MUSER system a key problem is that the high performance ultra-wide band feed is needed for reflecting antennas. Such feed should be with wide impedance bandwidth, low profile, symmetrical radiation patterns, and fixed phase center over whole band. Solar radio bursts and accordingly their polarizations vary quickly. Therefore, the isolation is important for correct observations of the polarizations. We have successfully developed the feeds for MUSER with VSWR less than 1.5 over most the frequency range and exhibits low profile, ultrawide impedance bandwidth and good radiation characteristics. It comes that in nearly 90% frequency band the polarization degree is less than 5%, which indicates good isolation performance [152, 153]. MUSER has been put into test observations and fixed time delays among MUSER-I array have been measured for calibration. The measured RMS variations for MUSER-I were < 1 ns which is very robust, as similar results obtained after multiple measurements pursued 1 years apart [154]. For the test observations, fringes of the satellite signals, the Sun, and Cygnus A have been obtained correctly for all baselines. The residuals of the phase closures for every tri-antenna composition were about 2 degrees for both geostationary and GPS satellites [155]. Whereas the residuals of the phase closures for every tri-antenna composition of MUSER-II were about 1 degree for geostationary satellites. These experiments have verified the system design and demonstrated the system performance. The two 20 m antennas in 400-1000 MHz will be incorporated into MUSER-I calibrations.

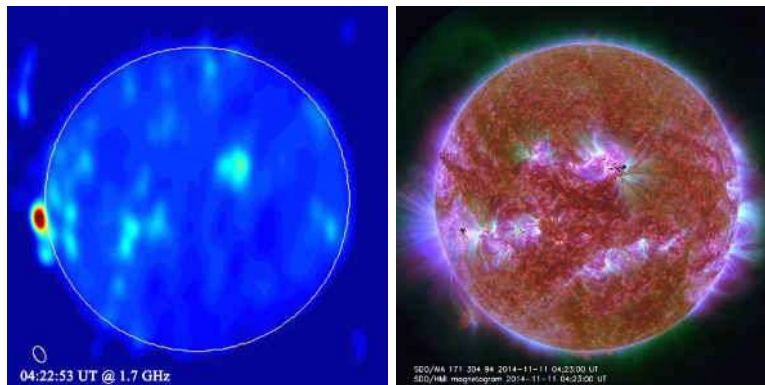


Fig 15. Radio image showing the peak burst source location (left panel) and composite AIA/SDO EUV image at several wavelengths (right panel).

On 11 Nov 2014, a radio burst event was registered by MUSER-I array at 400MHz-2GHz waveband. According to SGD event list there was a C-class flare peaked at 04:49 UT in the disk center and the radio bursts around 04:22-04:24 UT was attributed to this flare. However, MUSER-I imaging observation of the burst indicates that the radio burst peaked around 04:22 UT was due to the eruption at the east limb of the Sun. This demonstrates the importance of the image spectroscopy observation of the solar radio burst.

Figure 15 shows the radio image at burst peak from 1.7 GHz and the corresponding composite EUV image at 171 Å, 304 Å and 94 Å from AIA/SDO.

In summary, MUSER has the following merits: unique high resolution of time, space and frequency simultaneously over a wide wavelength range; innovative high performance ultra-wide-speed, large-scale digital correlation receiver implemented multi-frequency and snap-shot observations; and new technologies such as remote antenna and wide-band analog signal transmission through optical fibers. MUSER's capability of acquiring high temporal, spatial, and spectral resolution over a wide frequency range simultaneously will provide a new observational window on solar activities, such as flares and CMEs at radio wavelength. MUSER yields capability in measuring and imaging of magnetic fields from solar chromosphere to higher corona, helping us to understand the physics of various solar activities and the basic drivers of space weather. MUSER, as a new-generation radioheliograph, will be the major solar-dedicated leading radio facility in the world for solar physics.

3.3 AIMS (*Accurate Infrared Magnetic field Measurements of the Sun*)

Measuring magnetic field is the top priority in solar physics. In the measurement of solar magnetic field, spatial resolution and polarization accuracy are two of the most important parameters. In the past decades, methods and technologies for high spatial resolution observation enable us to approach the so-called "magnetic element" scale, i.e., the smallest spatial scale of basic magnetic structures.

However, the progress in high accurate polarimetry is limited in the past decades. The accuracy of magnetic measurement is far from satisfaction, especially for the transverse component. Even the best sensitivity currently obtained, a few Gauss, is not enough to detect the "background" solar magnetic field. Thus, no one knows what the weakest magnetic field is in the solar atmosphere. New technique is needed to improve this situation.

By means of mid-infrared spectral observation, one can get much larger Zeeman split. Thus, the strength of magnetic field may be directly "counted" from the quantity of line split. In this case, the sensitivity of magnetic measurement can be largely improved, as there is no "inversion" process need.

Based on this consideration, we have proposed a project to realize the "Accurate Infrared Magnetic field Measurements of the Sun", which is abbreviated as AIMS.

With a one-meter aperture, AIMS will concentrate on mid-Infrared observations. With very high spectral resolution (0.6 Å) and polarization accuracy (0.2%), AIMS can approach the sensitivity of 10 G for vector magnetic measurement. This enables us to directly observe the vector components of the ubiquitous weak solar magnetic fields.

The performances of AIMS are designed as follows:

- Working spectral line: Mg I 12.32 μm
- Detect sensitivity of magnetic field: 10 G
- Polarization Accuracy: $10^{-3} I_c$
- Spectral resolution: 0.6 Å with a customized IR FTS (FTIR)
- Diameter of telescope: 1 m
- Designed FOV: 192" × 192"
- Detector: 128×1 (present); 128×128 (expected in the future)
- Spatial resolution: 1.5" per pixel
- Temporal resolution: 30 s

The AIMS will also have a wide-band imager, which works at wavelength of 8-10 μm, with a FOV of 384" × 384", a 256 × 256 detector, and temporal resolution of 20 ms.

AIMS project has been approved by the National Natural Science Foundation of China in the end of 2014, with the budget of about 90 M RMB. The development period is from 2015 to 2019. Currently, we have finished basic optical design for AIMS (Fig 16), and it is proposed to be placed at Ali area of Tibet, western part of China [156]. This candidate is a good site for Infrared observation with the characteristics of high altitude (5100 m), long sunshine time, and low vapor.

3.4 Fiber Arrayed Solar Optic Telescope (FASOT): a solar spectro-imaging-polarimetric facility

FASOT is a specially-designed telescope dedicated to be a high-efficient polarimetry measurement with high polarimetric accuracy and high temporal resolution [157, 158]. We use fibers to feed polarimeter-processed focal plane light into the slits of a number of spectrographs. It is basically one of pre-research facilities to the future Chinese giant solar telescope. It is expected to be finished in 2020.

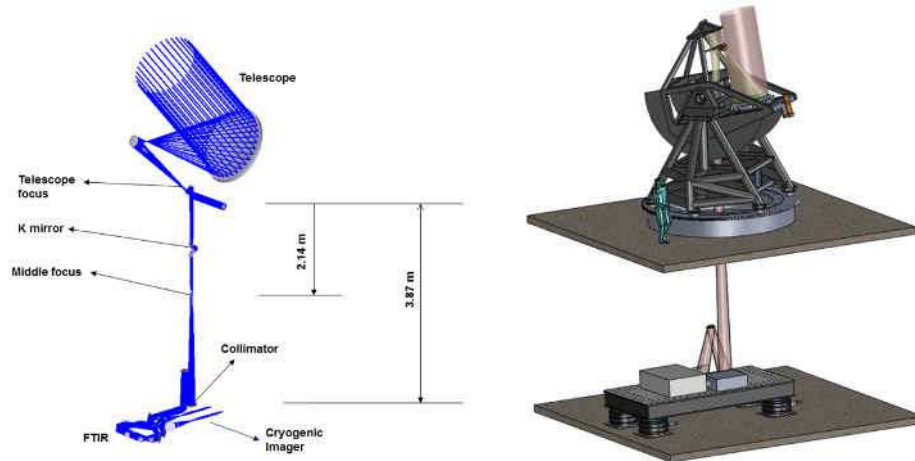


Fig 16. The optical design of AIMS.

FASOT is featured by real time spectro-imaging-polarimetry (imaging polarimetry available after spatially well-ordered 2-D spectropolarimetry by image reconstruction) of multiple lines forming in different depths in solar photosphere and chromosphere. This capacity is based on a couple of integral field units (IFUs), respectively, receiving co-spatially dual beams with opposite polarization states produced from a polarimeter with high polarimetric efficiency over the whole visible band. FASOT has been supported by Chinese solar physics community and sponsored by Natural Science Foundation of China (NSFC) under grant number 11527804. It is expected that she comes true in 2020.

The scientific objects are set to be as following: revealing the mechanisms of solar eruptions via tracking the transfer processes of matter and energy from photospheric bottom to the middle chromospheric layers at different height scales by mapping magnetic-field, line-of-sight velocity and thermodynamic parameters of 2-D spatial fields with high temporal resolution after Stokes spectrum inversion, i.e., stratifications of these physical parameters, searching for the fast variation, both cycling and non-cycling, related to magnetic field beyond the temporal resolutions of current instruments, and finally serving space weather broadcast after combination with other instruments with larger field of view.

In order to realize the above scientific objects, the observational goals should be achieved:

- Polarimetric accuracy: 8.0×10^{-4} ;
- Polarimetric sensitivity: 2.4×10^{-4} ;
- IFU FOV: 30 arcseconds by 30 arcseconds;

Temporal resolution of polarimetric modulation cycle: 3.0 s;
 Spatial resolution: 1.0" @525 nm;
 Spectral resolution power: 100,000@525 nm;
 Spectral window: 400 nm-1085 nm;
 The observational band of the first priority: 516.7 nm-525.1 nm.

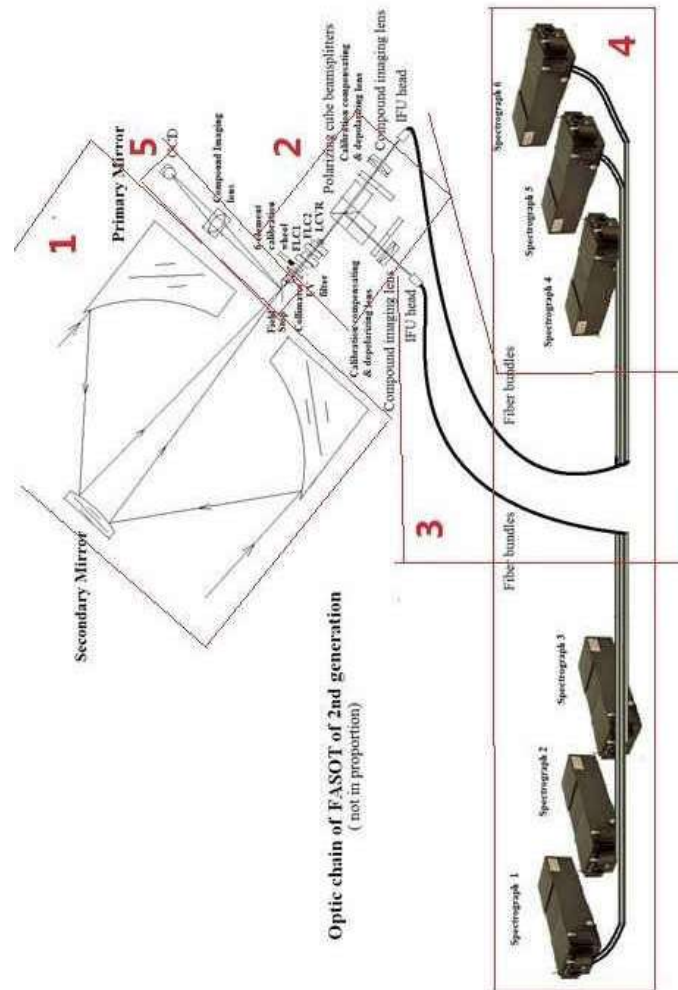


Fig 17. Optic chain of FASOT. Note that the parts are not plotted in equal scales.

The optic train of FASOT can be divided into five parts according to their positions in the optic train and functions (see Fig 17): the guiding optics of an RC system with an auto-guiding system, the polarimetric system producing two beams with opposite linear polarization states, a couple of IFUs, six IFU spectrographs and the monitoring system. The train owns the following features: 1) the polarimetry is immediately carried out after the guiding optics and no folding mirror before it, thus instrument-induced polarization can be ignored, and 2) optic-fiber-coupled lenslet with small numerical aperture is utilized to prevent the scattering and stray light. These layouts lay a basis for FASOT to achieve the high polarimetric accuracy.

3.5 Progress of solar site survey in western China

To build a large solar telescope with aperture size ranged about 5m - 8m and a large coronagraph with aperture of about 1m has been the consensus of Chinese solar physicists for developing their next-generation ground-based solar instruments since 2010. However, this puts very strict requirement for site conditions at the same time. Therefore, to find an excellent solar observation site in the western part of China is urgent at the first stage for the Chinese Giant Solar Telescope (CGST) project.

The remote investigations for the site survey task had been completed, based on comprehensive analysis of long-term meteorological data supplied by competent authorities, and the geological and geographic data collected from the geographic information system available.

We have made on-the-spot investigation for more than 50 different sites in western China with the help of remote survey results. The members of our site survey team come from a few institutes and universities including YNAO, NAOC, PMO, NJU and USTC. The site parameters containing average seeing factor r_0 , sky brightness, and precipitable water vapor content (PWVC) are used to exclude some obviously poor candidate sites. The instruments for the survey mainly contain standard solar differential image motion monitor (SDIMM), sky brightness monitor (SBM; [159]), PWVC monitor, DIMM, atmospheric temperature fluctuation monitor, robot weather station and so on. Strict calibrations for those instruments had been done carefully.



Fig 18. Bird view of Mt. Wumingshan (WMS) (E 100°04' 37", N 29°09' 07").

As an important progress, the Wumingshan (WMS) mountain of Sichuan (Fig 18) located in the Grand Shangri-La (GSL) area, in the bordering region of Tibet, Sichuan, Yunnan, Gansu and Qinghai, has been chosen to be one of the most potential regions worthy of further site survey for CGST. The atmosphere cleanliness in GSL is the most excellent in China, in terms of the global long-term average $PM_{2.5}$ concentrations and the average aerosol indexes deduced from satellite observations, and the average yearly sunshine duration for those regions is generally over 2500 hours [160]. The average altitude for GSL is around 3000 m above the sea level. One advantage of GSL is the large relative elevation difference in the terrain there, that is, we can not only find a place at a very high mountain for installing instruments but also can find a quite lower place with altitude of around 2000-3000 m for constructing headquarter and lodges of observatory within 100 km distance, which is critical for observers' health and convenient instrumental maintenance.

The average daily seeing factor of WMS is over 10 cm based on one-year measurements. Its average wind speed is less than 5 m s^{-1} . The average normalized PWVC at 1 air mass is about 3 mm. For WMS, cars can be directly driven to the top, which is one of the eminent advantages for WMS monitoring station to take successive site data. Figure 19 shows the WMS monitoring station running in winter snowing days.



Fig 19. The Wumingshan monitoring station in winter.

Based on the current data accumulated, the WMS site has been paid more and more attention for its excellent aspect in not only excellent daytime seeing condition but also for excellent night seeing. For the WMS station development, a new monitoring platform will be constructed at a location 7 km away in order to fully escape from evening light pollution from village, road and airport. The day-and-night continuous monitoring at WMS will be realized soon.

3.6 International collaborations

Chinese solar community constantly seeks international collaboration with oversea institutes and universities. All scholars in this community have the experience of academic exchange with foreign colleagues, either by short-term/long-term mutual visiting or bilateral/multilateral meetings. The APSPM series (Asia-Pacific Solar Physics Meeting) is a legacy from bilateral meetings between India, Korea and Japan. The 3rd APSPM was held in Seoul National University in November of 2015 with over 100 attendants. In the same year, supported by Sino-German Science Center (GZ1187), the 2nd international Sino-German Symposium on solar physics was held in Bad Honnef in August with the topic on multi-wavelength observations and modeling of solar activity. The bilateral meeting with Germany solar physicists, along with former series of Sino-France solar physics meeting, will develop into a larger Sino-Europe solar physics meeting, which forms another major academic exchange channel for Chinese solar community. Besides, we have held several special meetings/workshops for space missions like Hinode, RHESSI and SDO etc. In 2016, we will have an IRIS-7 workshop in Weihai in April with the main aim of educating students.

Chinese Academy of Sciences encourages international collaboration by establishing a variety of programs for all natural science disciplines. It offers a package of international fellowships, collectively called the “CAS President’s International Fellowship Initiative (PIFI)” to support highly-qualified international scientists and postgraduate students to work and study at CAS institutions and strengthen their scientific collaboration with CAS researchers. In the package, international scholars at nearly all levels, namely distinguished scientists, visiting scientists, postdoctoral researchers and PhD students, can find their appropriate positions. For example, distinguished scientists can be supported by The CAS President’s International Fellowship to conduct a lecture tour at CAS for 1-2 weeks. Each professor is invited to visit

at least two CAS-affiliated institutions (research institutes or universities) to lecture and interact with CAS researchers and postgraduate students. In 2015, Prof. Eric Priest was offered this kind of fellowship, he gave a series of wonderful lectures at Beijing, Kunming and Nanjing. During his visit, many researchers and postgraduate students benefited from his lectures and deep discussions with him.

In 2013, Chinese solar community initiates a five year facility-based collaboration with Big Bear Solar Observatory (BBSO) of New Jersey institute, which runs the 1.6 meter aperture solar telescope. The purpose of the collaboration is to exploit the scientific capabilities of the large aperture solar telescope, and by the way, to foster science for China's next generation large optical and infrared telescope. By contributing part of funds to BBSO toward technical development, overall efficient operation of NST and hosting Chinese solar astronomers, Chinese solar community obtains one month observation time each year. The collaboration is supported by the Strategic Priority Research Program of CAS. Starting at 2014, Chinese solar physicists have finished two-month observation with topics on Ellerman bombs, spicules, small-scale magnetic activities, sunspots and formation of filaments etc. Some outputs of the collaboration have appeared. For example, Su *et al* discovered that umbral waves rotates when they meet light bridges or twisted magnetic field lines, forming one-armed or multi-armed spiral structures [161] (Fig 20). Regarding the collaboration with BBSO, we will see more important scientific results in next few years by the collaborative studies.

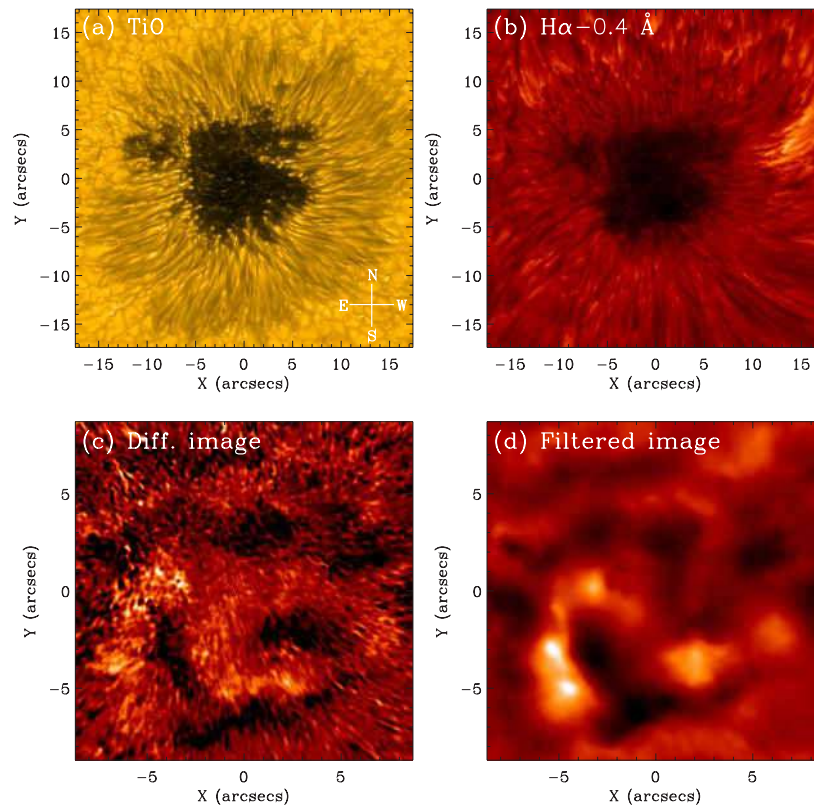


Fig 20. BBSO/NST observations of the umbral wavefronts with an evolving three-armed spiral that rotated clockwise, which will be published by a collaborative work led by Jiangtao Xu. Panels (a) and (b) TiO and H α maps of the sunspot in NOAA 12132 as observed on August 5, respectively. (c) the umbral wavefront detected with a difference method between two consecutive images. (d) the umbral wavefront detected with a phase-speed filtering method among a temporal sequence of images.

Nobeyama Radioheliograph (NoRH) is a radio interferometer specially designed to observe the full disk of the Sun at 17 and 34 GHz. NoRH continuously observes the full sun for about eight hours (22:30–6:30 UT) every day. The system has been quite stable and NoRH data are available in the period more than 99% out of the total possible operational window. The National Astronomical Observatory of Japan (NAOJ) had successfully operated NoRH during past two decades. Since April 2015, the International Consortium for the Continued Operation of Nobeyama Radioheliograph (ICCON) has been established to operate NoRH with the Institute for Space-Earth Environmental Research, Nagoya University as a representative of ICCON. ICCON consists of ISEE/Nagoya University, NAOC, KASI, NICT, and GSFC/NASA

4 Discussion on the future direction

For the past decades, we have seen a continuous increase in solar physics research groups in China. The growth was powered by the motivation for space weather forecasting and understanding the Sun's magnetism, by the domestic instrument development, and the availability of huge amount of high quality data from ground and especially from space. In the future, space weather forecast will become a fundamental need for a high-technology dependent society. Even so, we believe that the growth rate for the research team numbers in solar physics will finally reach a balance, and we need to develop novel ground- and space-based facilities in order to keep the team active and innovative. Meanwhile, with new facilities, we will have a largely increased and improved capability for space weather forecast. More contributions to the solar physics research, and even to other fields of astrophysics, will be made by solar physicists in China.

The long-suspending of Space Solar Telescope (SST) project, or the later-named Deep-space Solar Observatory (DSO) with a 1 meter solar optical telescope in space observations of vector magnetic field, has delayed the solar space projects in China. However, efforts have never been stopped for space-borne facilities for solar and space physics. The Advanced Solar Observatories (ASO), which consist of both ground-based and space-borne facilities: ASO-G [see, 162] and ASO-S [163-166] have been proposed. For ASO-G, we proposed an 8-meter aperture optical and infrared telescope, Chinese Giant Solar Telescope (CGST), and a large aperture coronagraph, Coronal Magnetism Telescopes of China (COMTEC), which aims at measuring the magnetic field in corona [167]. We carried out a systematic site survey and relevant instrumentation studies (for details, see Section 3.5).

ASO-S is a mission proposed for the 25th solar maximum by the Chinese solar community. The principle scientific goal is to study the relationship between solar magnetic field and two major types of solar activities: solar flares and coronal mass ejections (CMEs). As a small-size project, ASO-S consists of three payloads: Full-disk vector Magnetograph (FMG), Lyman-alpha Solar Telescope (LST, disc imager plus inner coronagraph), and Hard X-ray Imager (HXI, 30-300 keV). The objectives are to measure solar magnetic field, to observe CMEs (especially initiation and early transportation) and solar flares (mainly on non-thermal radiations), respectively. The ASO-S has been supported by the Strategic Pioneering Projects of Space Sciences sponsored by Chinese Academy of Sciences. We have finished its Phase-A study in 2013, and will finish its Phase-B study in early 2016. In late 2016, ASO-S have a chance to compete with other candidate missions for the engineering Phase-C study. If selected, ASO-S is expected to enter the whole engineering stage within 4 years, and to launch in 2021, so that it can cover the peak years of Solar Cycle 25.

Besides the above projects, another mission named LASGA, Large Area Solar Gamma-ray spectrometer, was proposed. The proposal was accepted by the Chinese Space Station. The energy range of LASGA is from 10 keV to 2.5 GeV. The geometry area is 4000 cm². As expected, LASGA could start its engineering study in 2016, it will be operated in space in 2020-2022. Considering the designed lifetime of 10 years, LASGA can observe ~500 solar gamma-ray line flares, ~10⁴ flares with X-ray class $\geq C$, ~10⁵ micro-flares and possibly nano-flares.

Due to the space weather and space climate effects, solar physics research has been developed beyond its traditional scope, being extended to the entire heliosphere. Its combination with space physics has already produced a new discipline: heliophysics. Heliosphere is a much larger and very complex region consisting of a variety of different physical features, with quite different spatial and temporal scales. One important scientific objective for heliophysics is to understand the cause-effect chain of mass and energy flow from the Sun through the entire heliosphere. No single instrument or institute can account for such a big task. From the observational point of view, we need enormous *in-situ* measurements as well as remote sensing. Under the framework of heliophysics, ASO will be an ingredient part of Heliophysics System Observatory. From the research point of view, solar physics teams should have more and more close and concrete collaborations with space physics teams. Actually, we have done so with a series of projects, under the name of national key basic research projects, sponsored by the Ministry of Science and Technology of China.

As we have mentioned above, Chinese solar physicists mostly focus on observational studies on solar magnetism, solar activity, coronal heating and solar wind, and solar activity monitoring and forecasting. Therefore, we must create theoretical tools and concepts for dealing with the large amount of observational data that are currently obtained and promoted for solar physics studies. We must foster abilities in building theoretical and numerical models. In particular, the three-dimensional radiative MHD simulations based on realistic solar atmosphere and radiation transfer models with observational input should be strongly encouraged. Meanwhile, to make progress in understanding turbulence and micro-instability in collisionless, hot and tenuous coronal plasma is a crucial task. Both will add knowledge to our understanding on the explosive release of magnetic energy in solar activity. We must establish new theoretical and numerical framework for forecasting space weather and make it operational based on achievements made in the last few decades [9].

Chinese solar physicists published a few hundred papers in the refereed research journals in the last three years. Among them, more than one hundred papers appeared in the *The Astrophysical Journal* (*Astrophys J*), accounting for over 1.3% of the total *Astrophys J* papers, or about 12% of the papers contributed by Chinese authors in this journal. We recognized that in quite many important areas, such as the solar interior and helioseismology, 3D radiative MHD simulation and modeling, Sun-as-a-star astrophysics, solar plasma physics and so on, we do not have very capable groups and have not made enough progress. Therefore, Chinese solar physicists need to catch up on and make desirable contributions to these interesting and increasingly important research fields in solar and heliospheric physics. As a summary remark, we shall work on the following urgent tasks in the near future: 1) to have the first Chinese space solar project founded and/or realized; 2) to make a detailed plan for the proposed CGST, including the selection of its final site; 3) to set up a capable research group working on the 3D radiative MHD simulations, supporting observational studies; 4) to deepen the observational studies with more quantitative results and physical insights. We believe that Chinese solar physicists can contribute to this branch of astrophysics in the world with increasingly influential works.

Acknowledgements

We are grateful to Xin Cheng, Yang Guo, Jiansen He, Zhenghua Huang, Jie Jiang, Chunlan Jin, Bo Li, Tong Shi, Jiangtao Su, Wei Su, Baolin Tan, Shangbin Yang, Qingmin Zhang, and Jinsong Zhao for providing part of the text, references and figures, and help in processing the manuscript. This work is supported by National Natural Science Foundation of China (NSFC) under grants 11333009, 11373023, 11427901, 11433006, 11527804, 11533009, 11573038 and 41474150. MUSER (CSRH) is supported by National Major Scientific Research Facility Program of China with the grant Number ZDYZ2009-3.

References

1. Ai G -X, Hu Y -F, *Acta Astron Sinica*, 27(1986)173-180.

2. Wang H, Zirin H, Patterson A, Ai G, Zhang H, *Astrophys J*, 343(1989)489-493.
3. Zhang H, Ai G, Sakurai T, Kurokawa H, *Solar Phys*, 136(1991)269-293.
4. Gu S M, Li B S, Ding Y J, Li S C, Li Z, *Solar Phys*, 87(1983)155-164.
5. Ye S -H, Jin J -H, *Solar Phys*, 96(1985)113-128.
6. Gan W -Q, Fang C, *Solar Phys*, 107(1987)311-321.
7. Ding M D, Fang C, *Astron Astrophys*, 225(1989)204-212.
8. Fang C, *Res Astron Astrophys*, 11(2011)1377-1402.
9. Wang J X, Ji H S, *Sci China: Earth Sci*, 56(2013)1091-1117.
10. Jiang C, Feng X, *Astrophys J*, 769(2013)144.
11. Jiang C, Wu S T, Feng X, Hu Q, *Astrophys J*, 780(2014)55.
12. Jiang C, Wu S T, Feng X, Hu Q, *Astrophys J Lett*, 786(2014)L16.
13. Wang R, Yan Y, Tan B, *Solar Phys*, 288(2013)507-529.
14. Jiang C, X. Feng, Wu S T, Q. Hu, *Astrophys J Lett*, 771(2013)L30.
15. Wang J X, Zhang Y Z, He H, Chen A Q, Jin C L, Zhao G P, *Sci China: Phys, Mech & Astron*, 58(2015)599601.
16. Jin C L, Harvey J W, Pietarila A, *Astrophys J*, 765(2013)79.
17. Yang S, Büchner J, Santos J C, Zhang H, *Solar Phys*, 283(2013)369-382.
18. Zhang H, Brandenburg A, Sokoloff D D, *Astrophys Lett J*, 784(2014)L45.
19. Zhang H, Yang S, *Astrophys J*, 763(2013)105.
20. Song Y L, Zhang M, *Astrophys J*, 804(2015)102.
21. Song Q, Zhang J, Yang S -H, Liu Y, *Res Astron Astrophys*, 13(2013)226-238.
22. Jin C L, Wang J X, *J Geophys Res*, 119(2014)11-17.
23. Jin C L, Wang J X, Song Q, Zhao H, *Astrophys J*, 731(2011)37.
24. Li K J, Kong D F, Liang H F, Feng W, *Astron Nach*, 335(2014)371-377.
25. Zhou G, Wang J, Jin C, *Solar Phys*, 283(2013)273-282.
26. Zhou G P, Wang J X, Jin C L, *Solar Phys*, 267 (2010)63-73.
27. Jin C L, Wang J X, *Astrophys J*, 806(2015)174.
28. Jin C L, Wang J X, *Astrophys J*, 807(2015)70.
29. Dikpati M, Gilman P A, *Astrophys J*, 649(2006)498-514.
30. Choudhuri A R, Chatterjee P, Jiang J, *Phys Rev Lett*, 98(2007)131103.
31. Jiang J, Chatterjee P, Choudhuri A R, *Mon Not Royal Astron Soc*, 381(2007)1527-1542.
32. Jiang J, Cameron R H, Schmitt D, Işık E, *Astron Astrophys*, 553(2013)A128.
33. Jiang J, Cameron R H, Schüssler M, *Astrophys J Lett*, 808(2015)L28.
34. Jiang J, Cameron R H, Schüssler M, *Astrophys J*, 791(2014)5.
35. Jiang J, Hathaway D H, Cameron R H, Solanki S K, Gizon L, Upton L, *Space Sci Rev*, 186(2014)491-523.
36. Li K J, Feng W, Shi X J, Xie J L, Gao P X, Liang H F, *Solar Phys*, 289(2014)759-768.
37. Li K J, Shi X J, Xie J L, Gao P X, Liang H F, Zhan L S, Feng W, *Mon Not Royal Astron Soc*, 433(2013)521-527.
38. Li K J, Xie J L, Shi X J, *Astrophys J Suppl*, 206(2013)15.
39. Yang S, Zhang J, Xiang Y, *Astrophys J Lett*, 798(2015)L11.
40. Sun J Q, Cheng X, Ding M D, Guo Y, Priest E R, Parnell C E, Edwards S J, Zhang J, Chen P F, Fang C, *Nat Commun*, 6(2015)7598.
41. Zhang J, Yang S, Li T, Zhang Y, Li L, Jiang C, *Astrophys J*, 776(2013)57.

42. Li T, Zhang J, *Astrophys J Lett*, 791(2014)L13.
43. Li T, Zhang J, *Astrophys J Lett*, 804(2015)L8.
44. Cheng X, Ding M D, Guo Y, Zhang J, Vourlidis A, Liu Y D, Olmedo O, Sun J Q, Li C, *Astrophys J*, 780(2014) 28.
45. Song H Q, Chen Y, Zhang J, Cheng X, Wang B, Hu Q, Li G, Wang Y M, *Astrophys J Lett*, 808(2015)L15.
46. Cheng X, Zhang J, Ding M D, Liu Y, Poomvises W, *Astrophys J*, 763(2013)43.
47. Cheng X, Zhang J, Ding M D, Olmedo O, Sun X D, Guo Y, Liu Y, *Astrophys J Lett*, 769(2013)L25.
48. Li T, Zhang J, *Astrophys J*, 770(2013)L25.
49. Yang S, Zhang J, Liu Z, Xiang Y, *Astrophys J Lett*, 784(2014)L36.
50. Liu Y D, Luhmann J G, Kajdivec P, Kilpua E K J, Lugaz N, Nitta N V, Möstl C, Lavraud B, Bale S D, Farrugia C J, Galvin A B, *Nat Commun*, 5(2014)3481.
51. Feng L, Wiegelmann T, Su Y, Inhester B, Li Y P, Sun X D, Gan W Q, *Astrophys J*, 765(2013)37.
52. Cheng X, Ding M D, Zhang J, Sun X D, Guo Y, Wang Y M, Kliem B, Deng Y Y, *Astrophys J*, 789(2014)93.
53. Cheng X, Ding M D, Fang C, *Astrophys J*, 804(2015)82.
54. Song H Q, Zhang J, Chen Y, Cheng X, *Astrophys J Lett*, 792(2014)L40.
55. Chen H, Zhang J, Cheng X, Ma S, Yang S, Li T, *Astrophys J Lett*, 797(2014)L15.
56. Ruan G, Chen Y, Wang S, Zhang H, Li G, Jing J, Su J, Li X, Xu H, Du G, Wang H, *Astrophys J*, 784(2014) 165.
57. Ruan G, Chen Y, Wang H, *Astrophys J*, 812(2015)120.
58. Yan X L, Xue Z K, Pan G M, Wang J C, Xiang Y Y, Kong D F, Yan L H, *Astrophys J Suppl*, 219(2015)17.
59. Shen Y, Liu Y D, Chen P F, Ichimoto K, *Astrophys J*, 795(2014)130.
60. Bi Y, Jiang Y, Yang J, Hong J, Li H, Yang D, Yang B, *Astrophys J*, 790(2014)100.
61. Chen P F, Harra L K, Fang C, *Astrophys J*, 784(2014)50.
62. Yan X L, Xue Z K, Liu J H, Ma L, Kong D F, Qu Z Q, Li Z, *Astrophys J*, 782(2014)67.
63. Chen H, Zhang J, Ma S, Yang S, Li L, Huang X, Xiao J, *Astrophys J Lett*, 808(2015)L24.
64. Zhang Q M, Ning Z J, Guo Y, Zhou T H, Cheng X, Ji H S, Feng L, Wiegelmann T, *Astrophys J*, 805(2015)4.
65. Hao Q, Fang C, Chen P F, *Sol Phys*, 286(2013)385-404.
66. Li D, Ning Z J, Zhang Q M, *Astrophys J*, 813(2015)59.
67. Li Y, Ding M D, Qiu J, Cheng J X, *Astrophys J*, 811(2015)7.
68. Dai Y, Ding M D, Guo Y, *Astrophys J Lett*, 773(2013)L21.
69. Liu K, Zhang J, Wang Y, Cheng X, *Astrophys J*, 768(2013)150.
70. Li Y, Ding M D, Guo Y, Dai Y, *Astrophys J*, 793(2014)85.
71. Zhang Q M, Chen P F, Guo Y, Fang C, Ding M D, *Astrophys J*, 746(2012)19.
72. Jiang F, Zhang J, Yang S, *Publ Astron Soc Jpn*, 67(2015)78.
73. Guo Y, Démoulin P, Schmieder B, Ding M D, Vargas Domínguez S, Liu Y, *Astron Astrophys*, 555(2013)A19.
74. Hong J -C, Jiang Y -C, Yang J -Y, Zheng R -S, Bi Y, Li H -D, Yang B, Yang D, *Res Astron Astrophys*, 13(2013) 253-258.
75. Zhang Q M, Ji H S, *Astron Astrophys*, 567(2014)A11.
76. Liu J, Wang Y, Shen C, Liu K, Pan Z, Wang S, *Astrophys J*, 813(2015)115.
77. Huang Z, Madjarska M S, Koleva K, Doyle J G, Duchlev P, Dechev M, Reardon K, *Astron Astrophys*, 566(2014) A148.
78. Tan B, Yan Y, Tan C, Sych R, Gao G, *Astrophys J*, 744(2012)166.
79. Tan B, Tan C, Zhang Y, Mészárosová H, Karlický M, *Astrophys J*, 780(2014)129.

80. Fu H S, Vaivads A, Khotyaintsev Y V, Olshevsky V, André M, Cao J B, Huang S Y, Retinò A, Lapenta G, *J Geophys Res Space*, 120(2015)3758-3782.
81. Yang K, Guo Y, Ding M D, *Astrophys J*, 806(2015)171.
82. Liu R, Titov V S, Gou T, Wang Y, Liu K, Liu J, Wang S, *Astrophys J*, 790(2014)8.
83. Zhao J, Li H, Pariat E, Schmieder B, Guo Y, Wiegelmenn T, *Astrophys J*, 787(2014)88.
84. Sun J Q, Cheng X, Guo Y, Ding M D, Li Y, *Astrophys J Lett*, 787(2014)L27.
85. Guo Y, Ding M D, Cheng X, Zhao J, Pariat E, *Astrophys J*, 779(2013)157.
86. Ni L, Kliem B, Lin J, Wu N, *Astrophys J*, 799(2015)79.
87. Ni L, Lin J, Mei Z, Li Y, *Astrophys J*, 812(2015)92.
88. Zhang Y Z, *Astrophys J*, 800(2015)43.
89. Zhang Q M, Chen P F, Xia C, Keppens R, Ji H S, *Astron Astrophys*, 554(2013)A124.
90. Li Y, Qiu J, Ding M D, *Astrophys J*, 781(2014)120.
91. Li L P, Peter H, Chen F, Zhang J, *Astron Astrophys*, 583(2015)A109.
92. Li B, Xie H, Li X, Xia L -D, in 8th Int Conf Num Model Space Plasma Flows, (eds) N V Pogorelov, E Audit, G P Zank, *Astron Soc Pacific Conf Ser*, 488(2014)155-160.
93. Huang Z, Xia L, Li B, Madjarska M S, *Astrophys J*, 810(2015)46.
94. Zhang Q M, Chen P F, Ding M D, Ji H S, *Astron Astrophys*, 568(2014)A30.
95. Mou C, Huang Z, Xia L, Madjarska M S, Li B, Fu H, Jiao F, Hou Z, *Astrophys J*, 818(2016)9.
96. Zhang Q M, Ji H S, *Astron Astrophys*, 557(2013)L5.
97. Hong J, Jiang Y, Yang J, Bi Y, Li H, Yang B, Yang D, *Astrophys J*, 796(2014)73.
98. Ning Z, Guo Y, *Astrophys J*, 794(2014)79.
99. Huang Z, Madjarska M S, Xia L, Doyle J G, Galsgaard K, Fu H, *Astrophys J*, 797(2014)88.
100. Yan Y, Peter H, He J, Tian H, Xia L, Wang L, Tu C, Zhang L, Chen F, Barczynski K, *Astrophys J*, 811(2015)48.
101. Zhang J, Zhang B, Li T, Yang S, Zhang Y, Li L, Chen F, Peter H, *Astrophys Lett J*, 799(2015)L27.
102. Yang L, He J, Peter H, Tu C, Zhang L, Feng X, Zhang S, *Astrophys J*, 777(2013)16.
103. Fu H, Xia L, Li B, Huang Z, Jiao F, Mou C, *Astrophys J*, 794(2014)109.
104. Su J T, *Astrophys J*, 793 (2014)117.
105. Jiao F, Xia L, Li B, Huang Z, Li X, Chandrashekar K, Mou C, Fu H, *Astrophys J Lett*, 809(2015)L17.
106. Shen Y -D, Liu Y, Su J -T, Li H, Zhang X -F, Tian Z -J, Zhao R -J, Elmhamdi A, *Sol Phys*, 288(2013)585-602.
107. Yang L, Zhang L, He J, Peter H, Tu C, Wang L, Zhang S, Feng X, *Astrophys J*, 800(2015)111.
108. Chen P F, Wu Y, *Astrophys J*, 732(2011)L20.
109. Shen Y, Ichimoto K, Ishii T T, Tian Z, Zhao R, Shibata K, *Astrophys J*, 786(2014)151.
110. Yang L, Zhang J, Liu W, Li T, Shen Y, *Astrophys J*, 775(2013)39.
111. Huang J, Tan B, Zhang Y, Karlicky M, Mészárosová H, *Astrophys J*, 791(2014)44.
112. Li D, Ning J Z, Zhang Q M, *Astrophys J*, 807(2015)72.
113. Chen S -X, Li B, Xiong M, Yu H, Guo M -Z, *Astrophys J*, 812(2015)22.
114. Guo M -Z, Chen S -X, Li B, Xia L -D, Yu H, *ArXiv e-prints*, (2015)1512.03692.
115. Yu S, Nakariakov V M, Selzer L A, Tan B, Yan Y, *Astrophys J*, 777(2013)159.
116. Guo Y, Erdélyi R, Srivastav A K, Hao Q, Cheng X, Chen P F, Ding M D, Dwivedi B N, *Astrophys J*, 799(2015)151.
117. Chen L, Wu D J, Huang J, *J Geophys Res Space*, 118(2013)2951-2957.
118. Chen L, Wu D J, Zhao G Q, Tang J F, Huang J, *Astrophys J*, 793(2014)13.
119. Wu D J, Chen L, *Astrophys J*, 771(2013)3.

120. Zhao J S, Wu D J, Lu J Y, *Astrophys J*, 767(2013)109.
121. Liu J, McIntosh S W, De Moortel I, Threlfall J, Bethge C, *Astrophys J*, 797(2014)7.
122. Zhao J S, Voitenko Y, Wu D J, De Keyser J, *Astrophys J*, 785(2014)139.
123. Zhao J S, Voitenko Y, De Keyser J, Wu D J, *Astrophys J*, 799(2015)222.
124. He J, Tu C, Marsch E, Bourouaine S, Pei Z, *Astrophys J*, 773(2013)72.
125. He J, Wang L, Tu C, Marsch E, Zong Q, *Astrophys J Lett*, 800(2015)L31.
126. He J, Pei Z, Wang L, Tu C, Marsch E, Zhang L, Salem C, *Astrophys J*, 805(2015)176.
127. Wang X, Tu C, He J, Marsch E, Wang L, *Astrophys J Lett*, 772(2013)L14.
128. Wang Y, Wei F S, Feng X S, Xu X J, Zhang J, Sun T R, Zuo P B, *Astrophys J Suppl*, 221(2015)34.
129. Wang X, Tu C, He J, Marsch E, Wang L, *Astrophys J Lett*, 783(2014)L9.
130. Wang X, Tu C, He J, Marsch E, Wang L, Salem C, *Astrophys J Lett*, 810(2015)L21.
131. Wang X, Tu C, Marsch E, He J, Wang L, *Astrophys J*, 816(2016)15.
132. Tang J, *Acta Astronom Sinica*, 55(2014)137-143.
133. Li K J, Feng W, Li F Y, *J Atmos Sol -Terr Phys*, 135(2015)72-76.
134. Miao J, Gong J, Li Z, T Ren, *Scientia Sinica Physica, Mechanica & Astronomica*, 45(2015)099601.
135. Du Z L, *Astrophys J*, 804(2015)3.
136. Liu X, Gong J, *Space Weather*, 13(2015)599-605.
137. Huang X, Zhang L, Wang H, Li L, *Astron Astrophys*, 549(2013)A127.
138. Li R, Zhu J, *Res Astron Astrophys*, 13(2013)1118-1126.
139. Yang X, Lin G, Zhang H, Mao X, *Astrophys J Lett*, 774(2013)L27.
140. He H, Wang H, Yan Y, Chen P F, Fang C, *J Geophys Res -Space*, 119(2014)3286-3315.
141. Dai X, Wang H, Huang X, Du Z, He H, *Astrophys J*, 780(2014)141.
142. Dai X, Wang H, Huang X, Du Z, He H, *Astrophys J*, 801 (2015) 39.
143. He H, Wang H, Yun D, *Astrophys J Suppl*, 221(2015)18.
144. Liu Z, Xu J, Gu B-Z, Wang S, You J-Q, Shen L-X, Lu R-W, Jin Z-Y, Chen L-F, Lou K, Li Z, Liu G-Q, Xu Z, Rao C-H, Hi Q-Q, Li R-F, Fu H-W, Wang F, Bao M -X, Wu M-C, Zhang B-R, *Res Astron Astrophys*, 14(2014) 705-718.
145. Lou K, Liu Z, Zhang R, Lu R, Wu M, *Prog Astron*, 19(2001)147-150.
146. Liu Z, Beckers J M, *Solar Phys*, 198(2001)197-209.
147. Wang R, Xu Z, Jin Z -Y, Li Z, Fu Y, Liu Z, *Res Astron Astrophys*, 13(2013)1240-1254.
148. Weigelt G P, *Opt Commun*, 21(1977)55-59.
149. Liu Z, Qiu Y, Lu R, in *Electronic Imaging and Multimedia Systems II*, 3561(1988)326-331.
150. Shen Y, Liu Y, Liu Y D, Chen P F, Su J, Hu Z, Liu Z, *Astrophys J Lett*, 814(2015)L17.
151. Yan Y, Wang W, Liu F, Geng L, Chen Z, Jian Z, in *Solar and Astrophysical Dynamos and Magnetic Activity*, eds. A G Kosovichev, E M de Gouveia Dal Pino, Y Yan, *Proc Int Astron Union*, 294(2013)489-494.
152. Li S, Yan Y H, Chen Z J, Wang W, Zhang F S, *Publ Astron Soc Aust*, 32(2015)e013(7 pages).
153. Li S, Yan Y -H, Chen Z -J, Wang W, Liu D -H, *Res Astron Astrophys*, 15(2015)1917.
154. Liu D-H, Yan Y -H, Zhao A, Wang W, *Acta Electron Sinica*, 41(2013)570-574.
155. Wang W, Yan Y, Liu D, Chen Z, Su, Liu F, Geng L, Chen L, Du J, *Publ Astron Soc Jpn*, 65(2013)S18.
156. Stone R, *Science*, 337(2012)1156-1157.
157. Qu Z Q, in *Solar Polarization 6*, (eds) J R Kuhn, D M Harrington, H Lin, S V Berdyugina, J Trujillo-Bueno, S L Keil, T Rimmele, *Astron Soc Pacific Conf Ser*, 437(2011)423-431.
158. Qu Z Q, Chang L, Cheng X M, Allington-Smith J, Murray G, Dun G T, in *Solar Polarization 7*, (eds) K N Nagendra,

- J O Stenflo, Z Q Qu, M Sampoorna, *Astron Soc Pacific Conf Ser*, 489(2014)263-270.
159. Zhao M Y, Liu Y, Elmhamdi A, Kordi A S, Al-trabulsy H A, Zhang X F, Song T F, Liu S Q, Shen Y D, Tian Z J, Miao Y H, *Mon Not Royal Astron Soc*, 443(2014)1955-1966.
160. Liu Y, Zhao L, *Mon Not Royal Astron Soc*, 434(2013)1674-1680.
161. Su J T, Ji K F, Banerjee D, Cao W D, Priya T G, Zhao J S, Yu S J, Ji H S, Zhang M, *Astrophys J*, 816(2016) 30.
162. Liu Z, Deng Y, Ji H, in Nature of Prominences and their role in Space Weather, (eds) B Schmieder, J-M Malherbe, S T Wu, *Proc Int Astron Union*, 300(2014)349-354.
163. Gan W, Huang Y, Yan Y, *Scientia Sinica Physica, Mechanica & Astronomica*, 42(2012)1274-1281.
164. Gan W, in 40th COSPAR Scientific Assembly, (2014) D2.3-14-14.
165. Gan W, *Chin J Space Sci*, 34(2014)563-564.
166. Gan W -Q, Feng L, *ISSI-BJ Magazine*, 5(2015)1-11.
167. Li H, Tomczyk S, in 40th COSPAR Scientific Assembly, (2014) E2.1-9-14.

[Received: 25.1.2016 ; accepted: 1.3.2016]